The official journal of the Japan Atherosclerosis Society and
the Asian Pacific Society of Atherosclerosis and Vascular Diseases

Original Article

J Atheroscler Thromb, 2026; 33: 809-834. http://doi.org/10.5551/jat.65991

A Single-Cell Analysis Reveals Macrophage Heterogeneity Driving Plaque Vulnerability in Coronary and Carotid Arteries

Takeshi Yoshida[1], Takuo Emoto[2], Hiroyuki Yamamoto[3], Tomofumi Takaya[3, 4], Takahiro Sawada[5], Sarah Louise Murphy[1, 6], Mitsuhiko Shoda[2], Keisuke Nakamura[2], Masayuki Taniguchi[7], Naoto Sasaki[8], Yuta Fukuishi[2], Takayoshi Toba[2], Takenao Ohkawa[9], Tomoyuki Furuyashiki[7], Hiroya Kawai[10], Ken-ichi Hirata[2, 5], Hiromasa Otake[2] and Tomoya Yamashita[1, 2]

[1]Division of Advanced Medical and Pharmaceutical Sciences, Graduate School of Science, Technology and Innovation, Kobe University, Kobe, Japan
[2]Division of Cardiovascular Medicine, Department of Internal Medicine, Kobe University Graduate School of Medicine, Kobe, Japan
[3]Division of Cardiovascular Medicine, Department of Internal Medicine, Hyogo Prefectural Harima-Himeji General Medical Center, Hyogo, Japan
[4]Division of Cardiovascular Medicine, Department of Exploratory and Advanced search in Cardiology, Kobe University Graduate School of Medicine, Kobe, Japan
[5]Division of Cardiovascular Medicine, Kakogawa Central City Hospital, Hyogo, Japan
[6]Research Institute of Internal Medicine, Oslo University Hospital, Oslo, Norway
[7]Division of Pharmacology, Kobe University Graduate School of Medicine, Kobe, Japan
[8]Laboratory of Medical Pharmaceutics, Kobe Pharmaceutical University, Kobe, Japan
[9]Department of Information and Intelligence Engineering, Kobe University, Kobe, Japan
[10]Division of Community Medicine and Health Science, Kobe University Graduate School of Medicine, Kobe, Japan

Aim: Acute coronary syndrome (ACS) and ischemic stroke are major life-threatening conditions caused by atherosclerosis. Although the mechanisms of atherosclerosis appear to be broadly similar across different vascular beds, growing evidence suggests that there are morphological and histological differences between coronary and carotid atherosclerosis. To identify disease-specific therapeutic strategies, we aimed to compare ACS and chronic coronary syndrome (CCS) in coronary artery disease, and symptomatic and asymptomatic carotid artery disease.

Methods: We analyzed our own single-cell RNA sequencing dataset for coronary artery disease (GSE184073) and a publicly available dataset for carotid artery disease (GSE253903). Myeloid cells were extracted from these datasets and comparative analyses were performed using metabolic profiling and an RNA velocity analysis.

Results: By integrating multiple velocity-inference approaches, including the original and dynamic RNA velocity models, TFvelo using transcription factor regulatory information, and CellRank, we consistently identified a differentiation trajectory toward interleukin-1B (IL1B)$^+$ inflammatory macrophages marked by high expression of matrix metalloproteinase 19 (MMP19). This trajectory was accompanied by the activation of the glycolytic and glycosaminoglycan degradation pathways. A similar directional flow toward IL1B$^+$ inflammatory macrophages was also observed in symptomatic carotid artery plaques. However, unlike coronary lesions, carotid lesions activated the glycolytic pathway in SPP1$^+$ foamy macrophages expressing MMP19.

Conclusions: Our findings revealed a shared differentiation trajectory into IL1B$^+$ inflammatory macrophages in carotid and coronary artery diseases, which is associated with plaque vulnerability. Notably, the distinct activation of the glycolytic pathway in a separate macrophage subset suggests that tailored therapeutic strategies may be necessary to effectively address plaque vulnerability in each vascular bed.

Key words: Coronary artery disease, Acute coronary syndrome, Carotid artery disease, Ischemic stroke, Single-cell RNA sequencing

Introduction:

Acute coronary syndrome (ACS) and ischemic stroke are the two major life-threatening complications of atherosclerosis. ACS, which encompasses acute myocardial infarction and unstable angina pectoris, causes primary ischemic cardiomyopathy and lethal arrhythmias. Ischemic stroke results from an abrupt interruption in the cerebral blood flow, leading to irreversible neuronal injury. Coronary artery disease, which underlies almost all cases of ACS, typically affects smaller arteries that are subjected to higher shear stress, making plaque rupture and thrombosis more likely. In contrast, carotid artery disease accounts for only approximately 20% of ischemic strokes; however, the risk of stroke generally increases with greater stenosis severity in symptomatic patients[1]. Despite advancements in the management of traditional risk factors such as dyslipidemia, diabetes, and hypertension, the incidence of plaque rupture has not been sufficiently prevented.

We previously characterized the immune cell composition of culprit coronary plaques responsible for ACS using single-cell RNA sequencing (scRNA-seq)[2]. Our analysis revealed a distinct immune landscape within myeloid cells in ACS plaques, including S100A8/9/12$^+$ monocytes, mast cells, and other immune cell populations. Notably, we identified chemokine (C-X-C motif) ligand 3 (CXCL3)$^+$ interleukin 1 B (IL1B)$^+$ inflammatory macrophages exclusively in the ACS plaques. Additionally, we found that the proportion of central memory cluster of differentiation (CD) 4$^+$ T cells was higher in ACS plaques[3].

Regarding carotid artery disease, another group demonstrated that plaque ruptures predominantly occur in the proximal and most stenotic regions rather than in the distal locations in the carotid plaques[4]. Proximal plaque locations have more immune cells, such as macrophages, T cells, B cells, and natural killer cells. In contrast, the distal locations contained more smooth muscle cells. Another study identified plaque-specific T cell populations exhibiting proatherogenic features[5].

Although the mechanisms of atherosclerosis appear to be broadly similar across different vascular beds, growing evidence suggests that there are morphological and histological differences between coronary and carotid atherosclerosis[6-8]. Virtual histology intravascular ultrasound studies comparing carotid and coronary plaques have shown that coronary arteries tend to have a higher amount of necrotic cores, whereas carotid arteries contain fibrofatty lesions[8]. A recent systematic review and meta-analysis demonstrated that the carotid lipid-rich necrotic core plaque phenotype is predictive of the early stages of coronary artery disease, whereas calcified carotid plaques are associated with more severe coronary artery disease[9]. Moreover, rupture-prone fibrous caps in coronary plaques are estimated to be as thin as 65μm, whereas in carotid plaques, vulnerability to plaque rupture and thrombosis occurs at a cap thickness of 200μm[6]. Recent clinical trials with anti-IL1B antibody (CANTOS) and colchicine (COLCOT and LoDoCO2) reduced cardiovascular events without lowering lipid levels in patients who were already receiving a full standard-of-care regimen, including high-dose statins, whereas effects on stroke were inconsistent (reduced in COLCOT as a secondary, unadjusted endpoint; not clearly reduced in CANTOS or LoDoCo2), suggesting differences in the pathophysiology[10-12]. Although these studies provide important insights into the different mechanisms of plaque progression across vascular beds in atherosclerotic diseases, comparative studies on the immune differences between these conditions remain limited. Therefore, it is necessary to understand how immune cells affect plaque vulnerability and to identify effective therapeutic targets for each disease.

In this study, we aimed to obtain valuable insights into the biological features of plaque vulnerability and inflammation common to and specific to lesion sites, and identify disease-specific therapeutic approaches by comparing ACS with chronic coronary syndrome (CCS) in coronary artery disease and asymptomatic and symptomatic cases of carotid artery disease within a unified analytical framework. Using scRNA-seq, we elucidated the immunological features that depend on the disease region and the mechanisms underlying plaque vulnerability, in terms of metabolism and cell differentiation.

Materials and Methods:

ScRNA-seq datasets of coronary artery plaques were collected from seven patients in a previous study (GSE184073)[2]. Viable CD45$^+$ immune cells were

Address for correspondence: Takuo Emoto, Division of Cardiovascular Medicine, Department of Internal Medicine, Kobe University Graduate School of Medicine, 7-5-1 Kusunoki-cho, Chuo-ku, Kobe 6500017, Japan E-mail: emotot@med.kobe-u.ac.jp

Received: August 27, 2025 Accepted for publication: January 12, 2026

sorted from three ACS plaques and four CCS plaques without high-intensity signals on T1-weighted magnetic resonance, which were obtained through directional coronary atherectomy. ScRNA-seq datasets for carotid artery plaques were obtained from public resources (GSE253903)[13]. These data were obtained from human carotid artery plaques collected from 18 patients who had undergone carotid endarterectomy. Patients were considered symptomatic if they had experienced a stroke or transient ischemic attack within six months of surgery. Patients without a history of ischemic events were classified as asymptomatic. The detailed methods for scRNA-seq, RNA velocity, Gene Ontology (GO) analyses, and metabolic analysis are described in the supplemental methods. The code is available at GitHub: https://github.com/Kobe-Cardiovascular/Single-cell-analysis-in-coronary-and-carotid-arteries.

Results:

Classification of Myeloid Cells in Coronary Plaques and Estimation of their Differentiation Direction by Single-cell RNA Sequencing

To elucidate the immunological features of coronary plaques, we focused on myeloid cells extracted from $CD45^+$ immune cells and performed an RNA velocity analysis using the scRNA-seq dataset (GSE184073) reported in our previous study[2].

The clustering of myeloid cells by uniform manifold approximation and projection (UMAP)[14] identified six distinct clusters in our previous study[2]: macrophages ($My^{Coronary\ (Co)}$.0, My^{Co}.1, My^{Co}.2), S100A8/9/12 monocytes (My^{Co}.3), mast cells and others (My^{Co}.4), and dendritic cells (My^{Co}.5). To distinguish the features of each macrophage cluster, we assigned functional designations as follows: My^{Co}.0 as "TNF^+ macrophages," My^{Co}.1 as "$C1Q^+$ $TREM2^+$ fibrotic macrophages," My^{Co}.2 as "$CXCL3^+$ $IL1B^+$ inflammatory macrophages," My^{Co}.3 as "S100A8/9/12 monocytes," My^{Co}.4 as "Mast cells and others," and My^{Co}.5 as "Dendritic cells" **(Fig. 1A and 1B)**.

A GO enrichment analysis supported these classifications **(Fig. 1C and Supplemental Fig. 1A)**. Gene Ontology-molecular function (GO-MF) revealed that cytokine, receptor-ligand, and signal receptor activator activities were prominent in My^{Co}.0 and My^{Co}.2 **(Fig. 1C)**. In contrast, My^{Co}.1 had a high expression related to not only extracellular matrix binding and the actin-binding functions in GO-MF, but also related to the collagen-containing extracellular matrix in the Gene Ontology-cellular component (GO-CC) **(Supplemental Fig. 1A)**. A Gene Ontology-Biological Process (GO-BP) analysis indicated that responses to interferon-γ and antigen processing and presentation were enriched in My^{Co}.0, whereas responses to oxygen levels and hypoxia were enriched in My^{Co}.2 **(Supplemental Fig. 1A)**. GO-CC analysis highlighted that My^{Co}.0 and My^{Co}.2 contained inflammatory cytokines in secretory granules and My^{Co}.1 promoted fibrosis by remodeling the extracellular matrix **(Supplemental Fig. 1A)**.

We performed an RNA velocity analysis using the velocyto.R[15] program to visualize the developmental lineages and cellular dynamics of macrophages by distinguishing between unspliced and spliced mRNAs **(Fig. 1D)**. TNF^+ macrophages (My^{Co}.0) and $C1Q^+$ $TREM2^+$ fibrotic macrophages (My^{Co}.1) largely retained their respective phenotypes in the CCS plaques. However, in ACS plaques, My^{Co}.0 and a small population of My^{Co}.1 were suspected to differentiate into $CXCL3^+$ $IL1B^+$ inflammatory macrophages (My^{Co}.2). To gain deeper insights into transcriptional factor-driven regulatory dynamics, we conducted an additional RNA velocity analysis using TFvelo[16], a method that leverages transcriptional factor expression levels rather than splicing kinetics, as in velocyto.R. TFvelo enables velocity estimation without requiring FASTQ files that contain splicing information. Consistent with the velocyto.R program, My^{Co}.0 in ACS plaques was again predicted to differentiate into My^{Co}.2, reinforcing the notion of an inflammatory shift unique to ACS lesions **(Fig. 1E)**. According to the learned weights of transcription factors, TFvelo showed that CEBPB, which has a reported relationship with atherosclerosis[17], is an important transcription factor for inflammatory shift because it has the highest weight **(Supplemental Fig. 2A and 2B)** and peudotime-aligned increase in expression levels **(Supplemental Fig. 3A and 3B)**. To provide an independent computational check, we conducted another velocity analysis using CellRank[18] and scVelo[19] (dynamical model), which supported an inflammatory shift unique to ACS lesions **(Supplemental Fig. 4A, 4C, and 5)**. These insights support those of a previous study that demonstrated that anti-inflammatory therapy with an antibody to IL1B, such as canakinumab, reduces the risk of recurrent cardiovascular events[20].

Active Metabolic Pathways and Expression of Genes Relevant to those Pathways with Myeloid Cells in Coronary Artery Disease

We performed a metabolic analysis at the single-cell level using scMetabolism[21], which visualized the activity of metabolic pathways based on the Kyoto Encyclopedia of Genes and Genomes (KEGG)[22]. Our analysis focused on five key pathways: oxidative

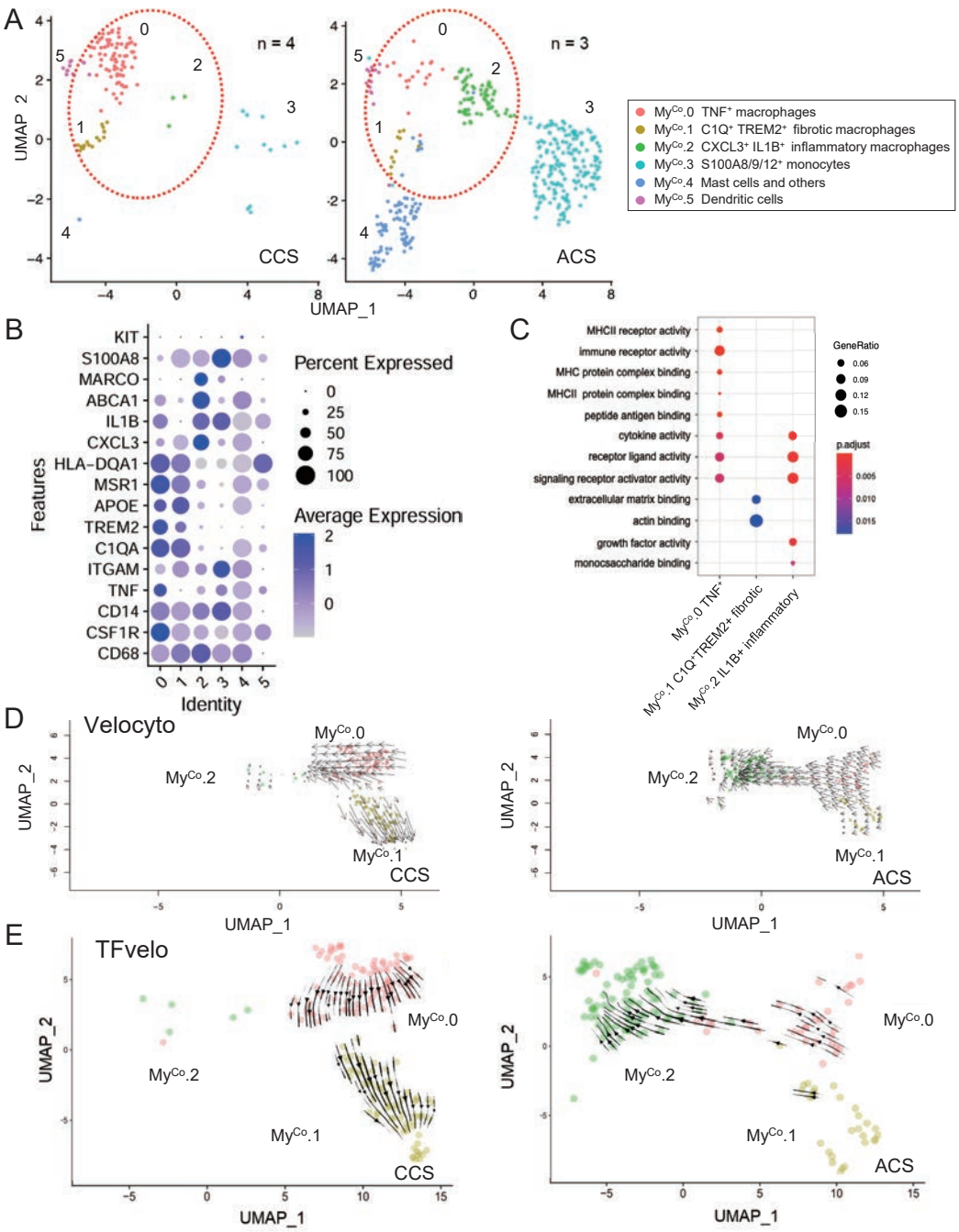

Fig. 1. A single-cell analysis reveals differentiation between acute coronary syndrome and chronic coronary syndrome in coronary plaques

A, Clustering of myeloid cells using Uniform Manifold Approximation and Projection (UMAP) separately for acute coronary syndrome (ACS, n = 3) and chronic coronary syndrome (CCS, n = 4). B, A Feature Dot plot depicting single-cell gene expression of each cell subset marker or important functional genes. C, Gene Ontology (GO) terms showing the enriched molecular function (MF) of each macrophage sub-cluster. D, A velocity stream plot by Velocyte. R with macrophage subclusters, separately for ACS and CCS. E, A velocity stream plot using TFvelo with macrophage subclusters, separately for ACS and CCS.

phosphorylation, glycosaminoglycan degradation, glycolysis/gluconeogenesis, fatty acid degradation, and tricarboxylic acid [TCA]) cycle. Among these pathways, oxidative phosphorylation, glycolysis/gluconeogenesis, fatty acid degradation, and the citrate cycle (TCA cycle) are central pathways related to adenosine triphosphate (ATP) production and cellular energy metabolism. Glycosaminoglycan degradation

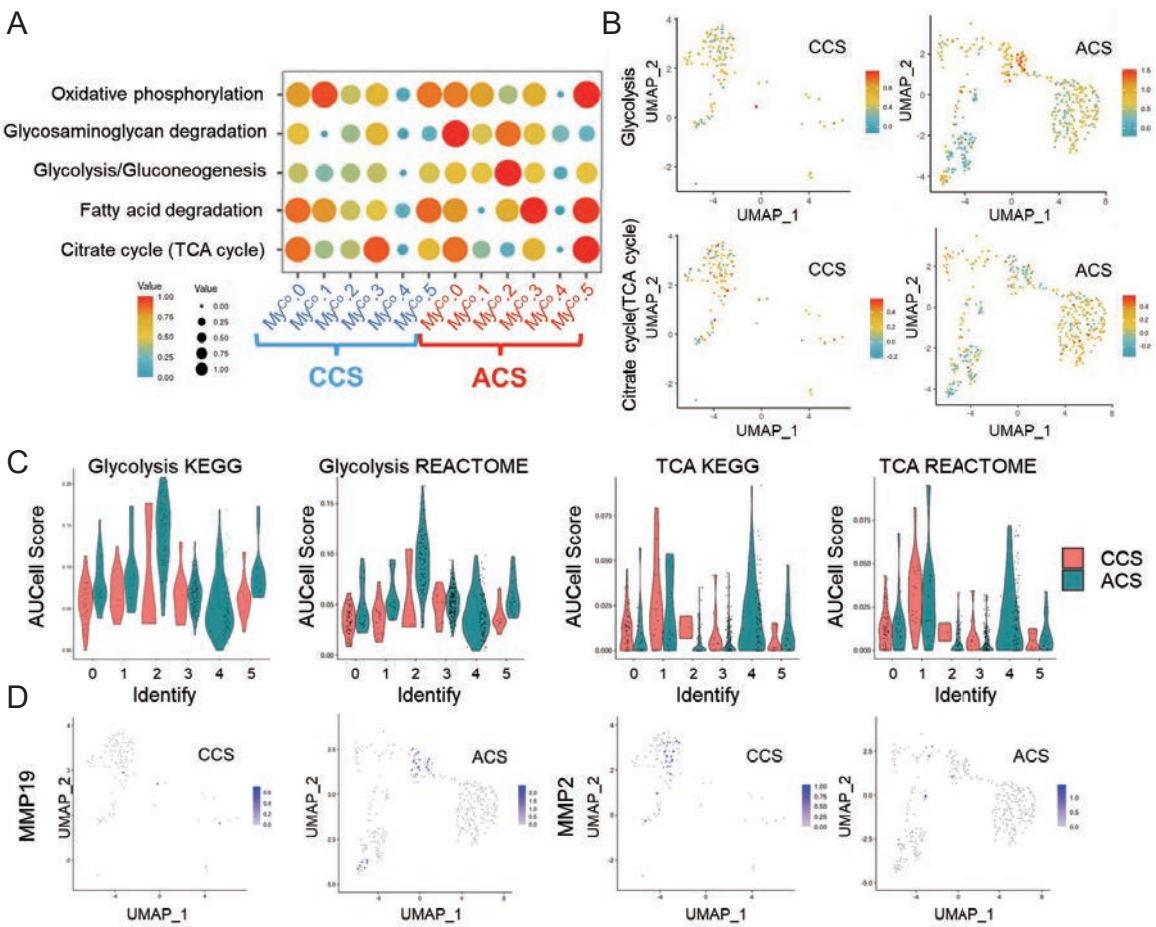

Fig. 2. A single-cell metabolic analysis reveals differentiation between acute coronary syndrome and chronic coronary syndrome in coronary plaques

A, Visualization of a metabolic analysis results of the KEGG pathways of interest by scMetabolism, separately for clusters in ACS and CCS on UMAP. B, A metabolic analysis of Glycolysis/Gluconeogenesis and Citrate cycle (TCA cycle) based on the KEGG by scMetabolism, visualized on UMAP, separately for ACS and CCS. C, AUCell-based visualization of glycolysis and citrate cycle (TCA) pathway activity using KEGG and Reactome gene sets, shown separately for ACS and CCS coronary plaques. D, A feature plot depicting the single-cell gene expression related to glycosaminoglycan degradation (MMP2, MMP19) on UMAP. The Wilcoxon rank-sum test with Bonferroni correction was performed between each gene expression in ACS and CCS. The q-value was significant for each comparison.

plays a critical role in extracellular matrix remodeling via the glycosaminoglycan uptake and degradation, a component of the extracellular matrix[23, 24].

To confirm the predicted metabolic shifts, we showed the expression of genes related to these metabolic pathways **(Supplemental Fig. 6A)** and performed computational cross-validation using AUCell[25] as an alternative scoring approach using both KEGG and Reactome[26] gene sets. The AUCell results were highly consistent with scMetabolism for glycolysis and the TCA cycle **(Fig. 2C)**, with the remaining three pathways shown in **Supplemental Fig. 7A and 7B**.

As shown in **Fig. 2A, 2B, and 2C**, glycolysis/gluconeogenesis was more active in ACS than in CCS, with a notable increase in My^{Co}.2 within ACS plaques, suggesting a heightened inflammatory response. Although oxidative phosphorylation and other canonical energy metabolism pathways were active in CCS-derived My^{Co}.0 and My^{Co}.1 clusters, as well as in their ACS counterparts, these pathways remained inactive in My^{Co}.2, underscoring a metabolic shift in inflammatory immune cells **(Fig. 2A, 2B, and 2C)**.

Importantly, the glycosaminoglycan degradation pathway was activated in My^{Co}.0 and My^{Co}.2 in ACS, but not in CCS-derived cells **(Fig. 2A)**. Among the various matrix metalloproteinases (MMPs)[27], a group of proteases that degrade the extracellular matrix and other substrates, MMP19 gene expression detected in My^{Co}.2 was specific to ACS plaques **(Fig. 2D)**. Additionally, MMP2, detected in My^{Co}.0, was strongly expressed in CCS plaques **(Fig. 2D)**. The expression

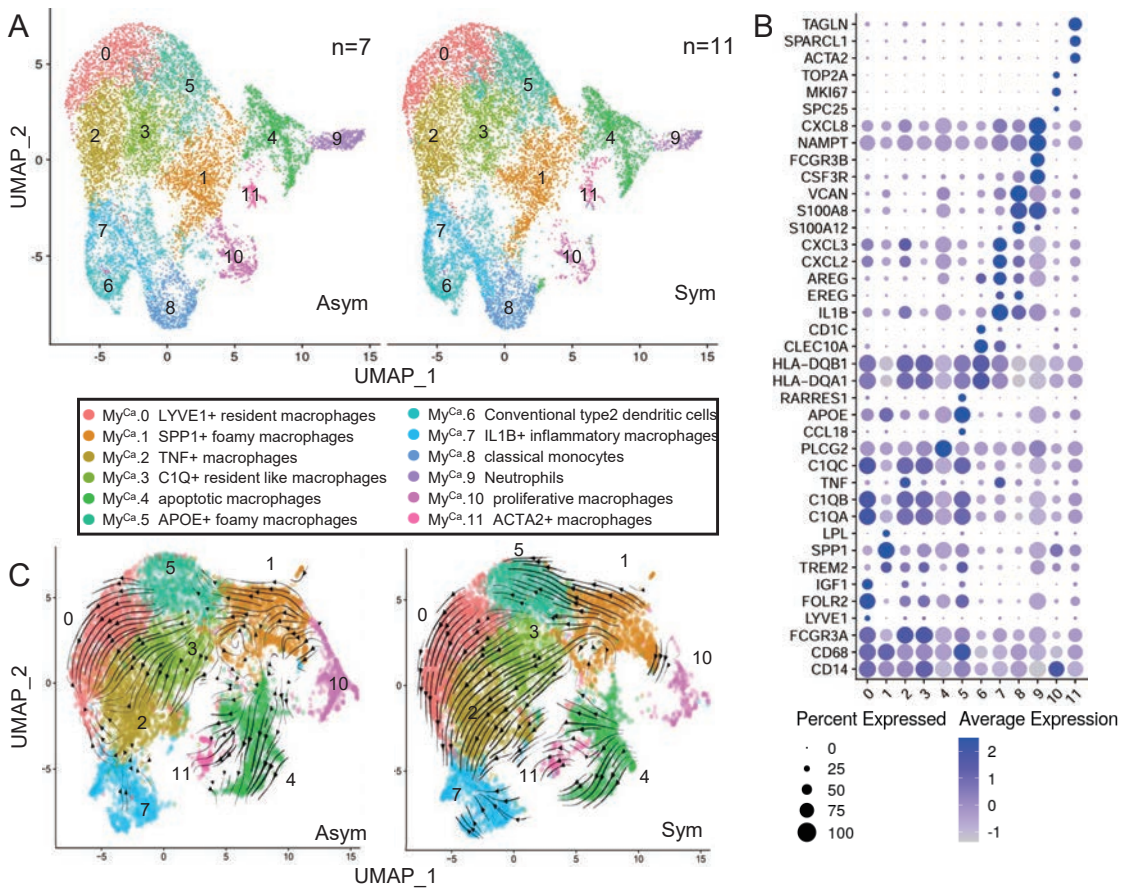

Fig. 3. A single-cell RNA sequencing analysis of myeloid cells in carotid artery plaques reveals differentiation between symptomatic and asymptomatic patients

A, Clustering of myeloid cells by Uniform Manifold Approximation and Projection (UMAP) separately for symptomatic carotid plaques (n = 11) and asymptomatic carotid plaques (n = 7). B, A Feature Dot plot depicting single-cell gene expression of each cell subset marker or important functional genes. C, The velocity stream plot projected onto the UMAP with macrophage subclusters, separately for symptomatic carotid plaques and asymptomatic carotid plaques. Macrophage subclusters were re-clustered after excluding the DC, neutrophil, and monocyte populations from all myeloid cell clusters.

of the other MMPs genes was not remarkable **(Supplemental Fig. 8A)**.

In addition, the expression of HIF1A, a regulator of glycolytic activation in proinflammatory macrophages[28, 29] is closely related to the activation of glycolysis in scmetabolism **(Supplemental Fig. 7C)**.

Classification of Myeloid Cells in Carotid Plaques and Estimation of their Differentiation Direction by Single-cell RNA Sequencing

To reveal the immunological features related to stroke in carotid plaques, we focused on myeloid cells extracted from the entire cell population and performed RNA velocity analysis using publicly available scRNA-seq data (GSE253903) from a previous study conducted by another group[13]. Because the clustering of myeloid cells was not discussed in detail, we re-clustered them, assigned functional annotations to each cluster, and examined their compatibility with coronary artery disease.

The re-clustering of myeloid cells using UMAP identified 12 distinct clusters: macrophages ($My^{Carotid\ (Ca)}$.0, My^{Ca}.1, My^{Ca}.2, My^{Ca}.3, My^{Ca}.4, My^{Ca}.5, My^{Ca}.7, My^{Ca}.10, and My^{Ca}.11), S100A8/9/12 monocytes (My^{Ca}.8), dendritic cells (My^{Ca}.6), and neutrophils (My^{Ca}.9). My^{Ca}.0, My^{Ca}.1, My^{Ca}.2, My^{Ca}.3, My^{Ca}.4, My^{Ca}.5, My^{Ca}.7, My^{Ca}.10, and My^{Ca}.11 were defined as macrophage clusters, expressing macrophage markers such as CD14, CD68, and CSF1R. My^{Ca}.8 was classified as a classical monocyte cluster owing to its high expression of monocyte markers, such as S100A8/9/12, a high expression of CD14, and low expression of CD16. My^{Ca}.6 was characterized by markers of conventional type 2 dendritic cells, including CLEC10A, FCER1A, and CD1C, although we could not detect DC1

populations. My^{Ca}.9 was characterized by neutrophil markers such as CXCL8 and FCGR3B **(Fig. 3A and 3B and Supplemental Fig. 9A and 9B)**.

Consistent with previous studies that analyzed myeloid cells in the heart or vasculature[30], My^{Ca}.0 was enriched in LYVE1 and FOLR2, which are markers of resident macrophages. My^{Ca}.2 and My^{Ca}.7 showed a high expression of proinflammatory cytokines, such as IL1B and TNF; chemokines, such as CXCL3 and CXCL8, which are suspected to regulate the migration of monocytes or neutrophils[31]; and toll-like receptors, with My^{Ca}.2, selectively expressing high levels of TNF and My^{Ca}.7 selectively expressing IL1B. My^{Ca}.1 and My^{Ca}.5 expressed foamy macrophages markers such as SPP1 and TREM2, but lacked proinflammatory gene expression; My^{Ca}.5 showed a higher expression of APOE and C1Q, and was similar to My^{Co}.1 in coronary artery disease, whereas My^{Ca}.1 showed a higher expression of SPP1 than My^{Ca}.5. To determine the differences between My^{Ca}.1 and My^{Ca}.5, we performed an additional differential gene expression (DEG) analysis **(Supplemental Fig. 9C)**. My^{Ca}.3 cells expressed high levels of C1Q and genes related to iron metabolism, such as FTL, suggesting that My^{Ca}.3 cells resemble intravascular macrophages reported in previous lung studies[32]. My^{Ca}.4 was enriched in apoptosis-related genes such as PLCG2. My^{Ca}.10 showed a high expression of genes related to cellular proliferation, including MKI67 and TOP2A, and its gene expression, including TREM2 and SPP1 expression levels, was similar to that of My^{Ca}.1, suggesting that My^{Ca}.10 might represent the proliferating cells of the My^{Ca}.1 lineage **(Fig. 3B and Supplemental Fig. 9B)**. My^{Ca}.11 expressed not only macrophage markers but also smooth muscle cell markers simultaneously, indicating that these cells may have undergone a phenotypic transition from smooth muscle to macrophage-like cells, as previously reported in this dataset[33] **(Fig. 3A and 3B and Supplemental Fig. 9A and 9B)**. To distinguish the features of each cluster, we specified functional designations as follows: My^{Ca}.0 as "$LYVE1^+$ resident macrophages," My^{Ca}.1 as "$SPP1^+$ foamy macrophages," My^{Ca}.2 as "TNF^+ macrophages," My^{Ca}.3 as "$C1Q^+$ resident like macrophages," My^{Ca}.4 as "apoptotic macrophages," My^{Ca}.5 as "$APOE^+$ foamy macrophages," My^{Ca}.6 as "Conventional type2 dendritic cells," My^{Ca}.7 as "$IL1B^+$ inflammatory macrophages," My^{Ca}.8 as "classical monocytes," My^{Ca}.9 as "Neutrophils," My^{Ca}.10 as "proliferative macrophages," and My^{Ca}.11 as "$ACTA2^+$ macrophages"**(Fig. 3A)**. No significant differences in percentages were observed between the carotid artery plaques in symptomatic and asymptomatic patients. Additionally, we performed a DEG analysis comparing symptomatic and asymptomatic samples and presented the results as a volcano plot **(Supplemental Fig. 10)**, indicating that myeloid cells as a whole in symptomatic plaques were more inclined toward inflammatory characteristics.

The GO enrichment analysis supported these classifications **(Supplemental Fig. 1B)**. A GO-MF analysis revealed strong cytokine and cytokine receptor-binding activities in My^{Ca}.2 and My^{Ca}.7 **(Supplemental Fig. 1B)**. In contrast, My^{Ca}.1 and My^{Ca}.5 showed enrichment in proteoglycan binding within the GO-MF, suggesting their involvement in tissue remodeling **(Supplemental Fig. 1B)**. A GO-BP analysis showed enrichment of antigen processing and presentation in My^{Ca}.0, My^{Ca}.2, My^{Ca}.3, and My^{Ca}.5, while My^{Ca}.10 displayed prominent nuclear division activity **(Supplemental Fig. 1B)**. A GO-CC analysis demonstrated enrichment of the collagen-containing extracellular matrix in My^{Ca}.1, My^{Ca}.5, and My^{Ca}.11 **(Supplemental Fig. 1B)**.

TFvelo was used to visualize the developmental lineages and cellular dynamics of the macrophages **(Fig. 3C)**. In asymptomatic plaques, a small subset of TNF^+ macrophages (My^{Ca}.2) and $C1Q^+$ resident-like macrophages (My^{Ca}.3) differentiate into $LYVE1^+$ resident macrophages (My^{Ca}.0). In contrast, in symptomatic plaques, My^{Ca}.0, My^{Ca}.2, and My^{Ca}.3 were predicted to differentiate into $IL1B^+$ inflammatory macrophages (My^{Ca}.7), a pattern similar to that observed in ACS plaques. In addition, $SPP1^+$ foamy macrophages (My^{Ca}.1) largely retained their phenotype in asymptomatic plaques, whereas they were predicted to differentiate into $APOE^+$ foamy macrophages (My^{Ca}.5) in symptomatic plaques. According to the learned weights of transcription factors, TFvelo showed that FOS, which has a reported relationship with inflammation in macrophages[34], is an important transcriptional factor for inflammatory shift because it has the highest weight **(Supplemental Fig. 2C and 2D)**. To provide an independent computational check, we conducted another velocity analysis using CellRank[18], which supported an inflammatory shift unique to asymptomatic patients **(Supplemental Fig. 4B)**. These results suggest that myeloid cells in symptomatic patients are more inclined to acquire inflammatory characteristics than myeloid cells in asymptomatic individuals, which is consistent with the dynamics observed in coronary plaques.

Active Metabolic Pathways and Gene Expression Relevant to those Pathways in Myeloid Cells in Carotid Artery Sclerosis

We performed a metabolic analysis of the single-

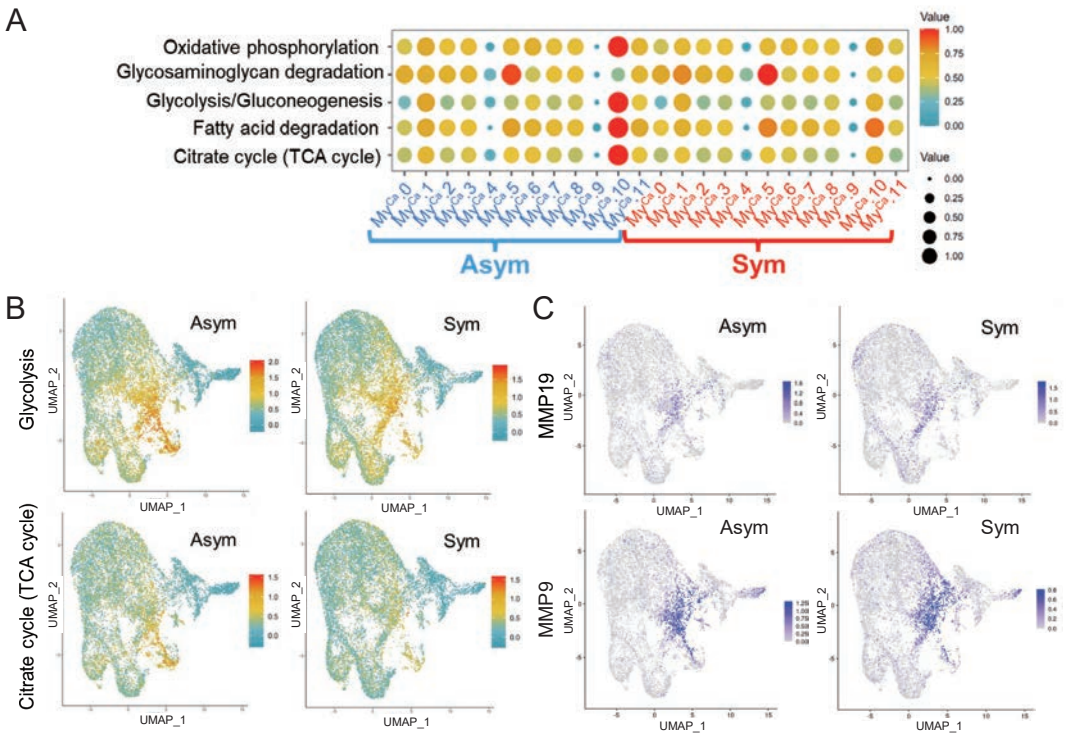

Fig. 4. A single-cell metabolic analysis of myeloid cells in carotid artery plaques reveals differences between coronary artery plaques and carotid artery plaques

A, Visualization of a metabolic analysis results of KEGG pathways of interest by scMetabolism, separately for clusters in symptomatic carotid plaques and asymptomatic carotid plaques on UMAP. B, A metabolic analysis of Glycolysis/Gluconeogenesis and Citrate cycle (TCA cycle) based on the KEGG by scMetabolism, visualized on UMAP, separately for symptomatic carotid plaques and asymptomatic carotid plaques. C, Feature plot depicting single-cell gene expression related to glycosaminoglycan degradation (MMP9, MMP19) on UMAP.

cell data from the carotid plaques **(Fig. 4A, 4B, and Supplemental Fig. 11A)**. To assess the robustness of the inferred metabolic shifts, we showed the expression of genes related to these metabolic pathways **(Supplemental Fig. 6B)** and conducted a computational cross-check by applying AUCell[25] with KEGG and Reactome[26] gene sets. The AUCell scores closely matched the scMetabolism results **(Supplemental Fig. 11B)**. Glycolysis/gluconeogenesis was activated in proliferating macrophages ($My^{Ca}.10$) and SPP1$^+$ foamy macrophages ($My^{Ca}.1$) in carotid plaques but not in IL1B$^+$ inflammatory macrophages ($My^{Ca}.7$), which were activated in coronary plaques **(Fig. 4A, 4B, and Supplemental Fig. 11A)**. Glycosaminoglycan degradation was strongly enhanced in APOE$^+$ foamy macrophages ($My^{Ca}.5$). There were no significant differences in metabolic activity between the carotid artery plaques in symptomatic and asymptomatic patients. MMP19 and MMP9 were more strongly expressed in $My^{Ca}.1$ than in $My^{Ca}.7$, in contrast to their expression in coronary plaques **(Fig. 4C)**. MMP14 was broadly expressed, whereas the other MMPs showed low or non-prominent expression **(Supplemental Fig. 8B)**.

In addition, the expression of SLC2A1 and MYC, regulators of glycolytic activation[28, 35], is closely related to the activation of glycolysis in the scMetabolism **(Supplemental Fig. 7D)**.

Discussion:

Our analyses revealed distinct heterogeneity in the cellular composition of the coronary and carotid atherosclerotic plaques. Further analysis, for the first time, demonstrated the differentiation trajectories and metabolic activity of myeloid cells in ACS and CCS plaques in coronary artery disease and in symptomatic and asymptomatic plaques in carotid artery disease. Notably, our velocity analysis revealed consistent trends in cellular differentiation across the coronary and carotid plaques, highlighting the potential shared mechanisms underlying plaque vulnerability. The distinct activation of the glycolytic pathway in separate macrophage subsets in coronary and carotid plaques suggests that tailored therapeutic strategies may be required to effectively address plaque progression in

each vascular bed.

Myeloid cells in coronary artery plaques can be subdivided into six types: macrophages, monocytes, mast cells, and dendritic cells. We previously performed a single-cell analysis of human coronary plaques and identified a significant population of CXCL3$^+$ IL1B$^+$ inflammatory macrophages (My^{Co}.2) in patients with ACS, highlighting the critical role of inflammatory macrophages in coronary artery plaques[2]. In the advanced analysis described in the current manuscript, we observed the differentiation of other cell types into CXCL3$^+$ IL1B$^+$ inflammatory macrophages, along with glycolytic metabolism, predominating the TCA cycle in these cells only in the ACS plaques. Glycolysis/gluconeogenesis synthesizes ATP, the energy currency, at a faster rate than other pathways by consuming large amounts of glucose, which is typically observed in cancer or inflammatory cells due to hypoxia and increased metabolic demands[36]. These findings reinforced the key role of inflammatory macrophages in the pathogenesis of ACS by supporting the result of a previous study demonstrating an increased uptake of fluorodeoxyglucose in the ACS plaques than in the CCS plaques[37].

Furthermore, our analysis revealed that glycosaminoglycan degradation in CXCL3$^+$ IL1B$^+$ inflammatory macrophages (My^{Co}.2) and TNF$^+$ macrophages (My^{Co}.0) was more active in ACS plaques than in CCS plaques. This suggests the potential contribution of these inflammatory cells to the destruction of coronary artery plaques in ACS. Next, we examined the gene expression of MMPs, the enzymes responsible for tissue destruction[27]. Previous studies have documented that MMPs appear to play dual beneficial and detrimental roles in atherosclerosis and have identified MMP1, MMP8, MMP12, MMP13, and MMP14 as proteinases associated with plaque vulnerability[38, 39], whereas another study documented that dysregulation of MMP2 led to plaque vulnerability in type 2 diabetes-associated atherosclerosis due to impaired fibrous cap formation[40]. In the present study, MMP19 detected in CXCL3$^+$ IL1B$^+$ inflammatory macrophages was highly expressed in patients with ACS, whereas MMP2 detected in TNF$^+$ macrophages was strongly expressed in patients with CCS. TNF$^+$ macrophages expressing MMP2 in CCS plaques may protect against atherosclerosis vulnerability by promoting fibrous cap formation. Regarding MMP19, no studies have directly linked MMP19 to plaque vulnerability or stabilization. However, MMP19 expression was higher in dilated aortas than in non-dilated aortas and potentially correlated with the maximal aortic diameter in patients with ascending aortic aneurysms[41]. Another study demonstrated that MMP19-mediated remodeling of the extracellular matrix in the central nervous system contributes to myelin sheath destruction in multiple sclerosis[42]. In addition, cell populations expressing MMP19 show high levels of glucose metabolism and glycosaminoglycan degradation in carotid and coronary artery diseases. These findings suggest that MMP19 plays a role in vascular tissue degradation and potentially contributes to plaque vulnerability in coronary artery disease. We suspect that metabolically active CXCL3$^+$ IL1B$^+$ inflammatory macrophages may contribute to plaque vulnerability by secreting MMP19 along with cytokines and chemokines such as CXCL3 and IL1B, although further experiments are required to confirm this.

Myeloid cells in carotid plaques were divided into 12 types: macrophages, monocytes, dendritic cells, and neutrophils, according to a previous study using the same data. IL1B-expressing inflammatory macrophages have been observed in carotid and coronary artery diseases, suggesting enriched inflammatory pathways in the process of atherosclerosis. Moreover, cellular differentiation predicted by TFvelo[16] revealed a differentiation flow from other clusters to IL1B$^+$ inflammatory macrophages only in symptomatic plaques. These findings highlight the important role of IL1B-expressing inflammatory macrophages in the vulnerability of both carotid and coronary plaques. However, we observed a different feature of IL1B$^+$ inflammatory macrophages compared to coronary artery disease, specifically deactivated glycolytic metabolism in carotid IL1B$^+$ inflammatory macrophages (My^{Ca}.7). In contrast, SPP1$^+$ foamy macrophages (My^{Ca}.1) showed activated glycolysis, whereas APOE$^+$ foamy macrophages (My^{Ca}.5) exhibited activated glycosaminoglycan degradation in the carotid plaques. Both macrophage populations highly expressed TREM2, suggesting that APOE$^+$ foamy macrophages with a high expression of TREM2 and C1Q were similar to the C1Q$^+$ TREM2$^+$ fibrotic macrophages found in coronary plaques. However, the exact function of TREM2 remains to be elucidated. One study demonstrated that TREM2-expressing macrophages help maintain the balance between foam cell death and clearance of dead cells in atherosclerotic lesions by expressing LPL, APOE, and LIPA, thereby promoting the cholesterol metabolism and suppressing inflammation. In contrast, another study reported that macrophage-specific Trem2 deletion in mice delayed atherosclerosis progression and reduced the plaque burden by downregulating cholesterol efflux molecules

in macrophages, resulting in weakened proliferation and survival[43]. We also demonstrated that monocyte-derived Trem2$^+$ macrophages mediate vascular damage and aneurysm development in a novel cigarette smoke-exposed aortic aneurysm murine model[44].

SPP1 promotes inflammation in atherosclerotic plaques, leading to increased proliferation and migration of smooth muscle cells[45]. Additionally, we observed high expression of MMP9, which was indicated as "anti-inflammatory gene"[39, 46], and MMP19 in SPP1$^+$ foamy macrophages. Therefore, SPP1$^+$ foamy macrophages have controversial features that promote or prevent the development of atherosclerosis. The activation of glycolysis in SPP1$^+$ foamy macrophages (My^{Ca}.1) indicated that these cells play a major role in carotid artery disease. In the present study, we did not observe any differences in SPP1$^+$ foamy macrophages between symptomatic and asymptomatic carotid artery plaques, suggesting that these macrophages may contribute to atherosclerosis progression in carotid plaques rather than directly driving plaque vulnerability and symptomatic events, such as brain infarction.

APOE$^+$ foamy macrophages (My^{Ca}.5) showed moderate expression of inflammatory genes such as C1Q and genes related to lipid metabolism such as APOE and TREM2. Our analysis revealed a differentiation pathway from SPP1$^+$ foamy macrophages to APOE$^+$ foamy macrophages that exhibited inflammatory gene expression and activated the glycosaminoglycan degradation pathway. A previous study indicated that C1Q, which has both proatherogenic and antiatherogenic effects, is involved in atherosclerosis progression and plaque instability by weakening the antiatherogenic effects in advanced lesions[47], highlighting the contribution of APOE$^+$ foamy macrophages expressing C1Q to atherosclerotic plaque vulnerability. We suspect that these differentiation trajectories into macrophages with inflammatory properties in ACS and symptomatic plaques may be common features of unstable plaques, resulting in vascular events.

There are also some limitations associated with this study. First, it was difficult to obtain sufficient cells, especially for minor cell populations, because of the small sample size obtained using DCA. Second, in the public scRNA-seq datasets of carotid artery disease, patients without a history of ischemic events were defined as asymptomatic. Consequently, some asymptomatic patients may have unstable plaques, potentially explaining the minimal differences observed in the cellular composition and metabolic activity between asymptomatic and symptomatic patients. Third, the evidence level is limited because the findings rely primarily on single-cell RNA-seq without orthogonal validation (e.g., immunostaining of plaques from several ACS and CCS patients), and these results should be regarded as hypothesis-generating, and mechanistic/therapeutic interpretations should be tempered. Fourth, owing to sample constraints, our ability to evaluate inter-individual variation is limited.

In summary, we identified a shared differentiation trajectory in IL1B-expressing inflammatory macrophages in the vascular regions associated with plaque vulnerability. In contrast, glycolysis is predominant in CXCL3$^+$ IL1B$^+$ inflammatory macrophages specific to ACS in coronary artery plaques, but in SPP1$^+$ foamy macrophages in carotid artery plaques. These findings suggest that proinflammatory cytokines (e.g., IL1B) might be effective therapeutic targets to reduce plaque vulnerability, whereas different therapeutic target cells should be considered for each disease: CXCL3$^+$ IL1B$^+$ inflammatory macrophages in ACS and SPP1$^+$ foamy macrophages in carotid artery disease.

Conflict of Interest

None.

Acknowledgements and Notice of Grant Support

Funding: This study was supported by the Japan Society for the Promotion of Science KAKENHI (Grant No. 24K02448 to T.E., 23H02905 to K.H., 24K02447 to T.Y., 21H04812 to T.F.), the Japan Agency for Medical Research and Development (JP23tm0724607 to K.H., JP24wm0425001, JP24zf0127010, JP24zf0127012 to T.F., and JP24ek0109755 to T.Y.), Grants-in-Aid for Scientific Research from the Ministry of Education, Culture, Sports, Science and Technology in Japan (JP21H04812, JP24K22086 to T.F.), Japan Science and Technology Agency (JPMJMS239F to T.F.), Uehara Memorial Foundation to T.E., Naito Foundation to T.E., Cardiovascular Research Fund to T.E., MSD Life Science Foundation to T.E., Chugai Foundation for Innovative Drug Discovery Science to T.E, Takeda Science Foundation to T.E., Japan Heart Foundation to T.E., Senshin Medical Research Foundation to T.E., and Astellas Foundation for Research on Metabolic Disorders to T.Y.

References:

1) Musialek P, Bonati LH, Bulbulia R, Halliday A, Bock B,

Capoccia L, Eckstein H-H, Grunwald IQ, Lip PL, Monteiro A, Paraskevas KI, Podlasek A, Rantner B, Rosenfield K, Siddiqui AH, Sillesen H, Van Herzeele I, Guzik TJ, Mazzolai L, Aboyans V, and Lip GYH: Stroke risk management in carotid atherosclerotic disease: a clinical consensus statement of the ESC Council on Stroke and the ESC Working Group on Aorta and Peripheral Vascular Diseases. Cardiovascular Research, 2025; 121: 13-43

2) Emoto T, Yamamoto H, Yamashita T, Takaya T, Sawada T, Takeda S, Taniguchi M, Sasaki N, Yoshida N, Saito Y, Sivasubramaniyam T, Otake H, Furuyashiki T, Robbins CS, Kawai H, and Hirata K: Single-Cell RNA Sequencing Reveals a Distinct Immune Landscape of Myeloid Cells in Coronary Culprit Plaques Causing Acute Coronary Syndrome. Circulation, 2022; 145: 1434-1436
3) Takeda S, Emoto T, Yamashita T, Yamamoto H, Takaya T, Sawada T, Yoshida T, Inoue M, Suzuki Y, Hamana T, Inoue T, Taniguchi M, Sasaki N, Otake H, Ohkawa T, Furuyashiki T, Kawai H, and Hirata K: Single-Cell RNA Sequencing Reveals an Immune Landscape of $CD4^+$ T Cells in Coronary Culprit Plaques With Acute Coronary Syndrome in Humans. ATVB, 2024; 44: 1135-1143
4) Sun J, Singh P, Shami A, Kluza E, Pan M, Djordjevic D, Michaelsen NB, Kennbäck C, Van Der Wel NN, Orho-Melander M, Nilsson J, Formentini I, Conde-Knape K, Lutgens E, Edsfeldt A, and Gonçalves I: Spatial Transcriptional Mapping Reveals Site-Specific Pathways Underlying Human Atherosclerotic Plaque Rupture. Journal of the American College of Cardiology, 2023; 81: 2213-2227
5) Tan J, Liang Y, Yang Z, He Q, Tong J, Deng Y, Guo W, Liang K, Tang J, Shi W, and Yu B: Single-Cell Transcriptomics Reveals Crucial Cell Subsets and Functional Heterogeneity Associated With Carotid Atherosclerosis and Cerebrovascular Events. ATVB, 2023; 43: 2312-2332
6) Virmani R, Ladich ER, Burke AP, and Kolodgie FD: Histopathology of Carotid Atherosclerotic Disease. Neurosurgery, 2006; 59: S3-219-S3-227
7) Sakakura K, Nakano M, Otsuka F, Ladich E, Kolodgie FD, and Virmani R: Pathophysiology of Atherosclerosis Plaque Progression. Heart, Lung and Circulation, 2013; 22: 399-411
8) Sondore D, Trušinskis K, Linde M, Briede I, Narbute I, Jēgere S, Griķis K, Štrenge K, and Ērglis A: Association between carotid and coronary atherosclerotic plaque morphology: a virtual histology intravascular ultrasound study. J Clin Transl Res, 2023; 9: 253-260
9) Bytyçi I, Shenouda R, Wester P, and Henein MY: Carotid Atherosclerosis in Predicting Coronary Artery Disease: A Systematic Review and Meta-Analysis. ATVB, 2021; 41
10) Ridker PM, Everett BM, Thuren T, MacFadyen JG, Chang WH, Ballantyne C, Fonseca F, Nicolau J, Koenig W, Anker SD, Kastelein JJP, Cornel JH, Pais P, Pella D, Genest J, Cifkova R, Lorenzatti A, Forster T, Kobalava Z, Vida-Simiti L, Flather M, Shimokawa H, Ogawa H, Dellborg M, Rossi PRF, Troquay RPT, Libby P, and Glynn RJ: Antiinflammatory Therapy with Canakinumab for Atherosclerotic Disease. N Engl J Med, 2017; 377: 1119-1131
11) Tardif J-C, Kouz S, Waters DD, Bertrand OF, Diaz R, Maggioni AP, Pinto FJ, Ibrahim R, Gamra H, Kiwan GS, Berry C, López-Sendón J, Ostadal P, Koenig W, Angoulvant D, Grégoire JC, Lavoie M-A, Dubé M-P, Rhainds D, Provencher M, Blondeau L, Orfanos A, L'Allier PL, Guertin M-C, and Roubille F: Efficacy and Safety of Low-Dose Colchicine after Myocardial Infarction. N Engl J Med, 2019; 381: 2497-2505
12) Nidorf SM, Fiolet ATL, Mosterd A, Eikelboom JW, Schut A, Opstal TSJ, The SHK, Xu X-F, Ireland MA, Lenderink T, Latchem D, Hoogslag P, Jerzewski A, Nierop P, Whelan A, Hendriks R, Swart H, Schaap J, Kuijper AFM, Van Hessen MWJ, Saklani P, Tan I, Thompson AG, Morton A, Judkins C, Bax WA, Dirksen M, Alings M, Hankey GJ, Budgeon CA, Tijssen JGP, Cornel JH, and Thompson PL: Colchicine in Patients with Chronic Coronary Disease. N Engl J Med, 2020; 383: 1838-1847
13) Bashore AC, Yan H, Xue C, Zhu LY, Kim E, Mawson T, Coronel J, Chung A, Sachs N, Ho S, Ross LS, Kissner M, Passegué E, Bauer RC, Maegdefessel L, Li M, and Reilly MP: High-Dimensional Single-Cell Multimodal Landscape of Human Carotid Atherosclerosis. ATVB, 2024; 44: 930-945
14) Becht E, McInnes L, Healy J, Dutertre C-A, Kwok IWH, Ng LG, Ginhoux F, and Newell EW: Dimensionality reduction for visualizing single-cell data using UMAP. Nat Biotechnol, 2019; 37: 38-44
15) La Manno G, Soldatov R, Zeisel A, Braun E, Hochgerner H, Petukhov V, Lidschreiber K, Kastriti ME, Lönnerberg P, Furlan A, Fan J, Borm LE, Liu Z, Van Bruggen D, Guo J, He X, Barker R, Sundström E, Castelo-Branco G, Cramer P, Adameyko I, Linnarsson S, and Kharchenko PV: RNA velocity of single cells. Nature, 2018; 560: 494-498
16) Li J, Pan X, Yuan Y, and Shen H-B: TFvelo: gene regulation inspired RNA velocity estimation. Nat Commun, 2024; 15: 1387
17) Rahman SM, Baquero KC, Choudhury M, Janssen RC, De La Houssaye BA, Sun M, Miyazaki-Anzai S, Wang S, Moustaid-Moussa N, Miyazaki M, and Friedman JE: C/EBPβ in bone marrow is essential for diet induced inflammation, cholesterol balance, and atherosclerosis. Atherosclerosis, 2016; 250: 172-179
18) Weiler P, Lange M, Klein M, Pe'er D, and Theis F: CellRank 2: unified fate mapping in multiview single-cell data. Nat Methods, 2024; 21: 1196-1205
19) Bergen V, Lange M, Peidli S, Wolf FA, and Theis FJ: Generalizing RNA velocity to transient cell states through dynamical modeling. Nat Biotechnol, 2020; 38: 1408-1414
20) Ridker PM, Everett BM, Thuren T, MacFadyen JG, Chang WH, Ballantyne C, Fonseca F, Nicolau J, Koenig W, Anker SD, Kastelein JJP, Cornel JH, Pais P, Pella D, Genest J, Cifkova R, Lorenzatti A, Forster T, Kobalava Z, Vida-Simiti L, Flather M, Shimokawa H, Ogawa H, Dellborg M, Rossi PRF, Troquay RPT, Libby P, and Glynn RJ: Antiinflammatory Therapy with Canakinumab for Atherosclerotic Disease. N Engl J Med, 2017; 377: 1119-1131
21) Wu Y, Yang S, Ma J, Chen Z, Song G, Rao D, Cheng Y, Huang S, Liu Y, Jiang S, Liu J, Huang X, Wang X, Qiu S,

Xu J, Xi R, Bai F, Zhou J, Fan J, Zhang X, and Gao Q: Spatiotemporal Immune Landscape of Colorectal Cancer Liver Metastasis at Single-Cell Level. Cancer Discovery, 2022; 12: 134-153
22) Kanehisa M, and Goto S: KEGG: Kyoto Encyclopedia of Genes and Genomes. Nucleic Acids Research, 1999; 27: 29-34
23) Fuchs W, Beck M, and Kresse H: Intralysosomal formation and metabolic fate of N-acetylglucosamine 6-sulfate from keratan sulfate. Eur J Biochem, 1985; 151: 551-556
24) Greiling H, Stuhlsatz HW, Cantz M, and Gehler J: Increased urinary excretion of keratan sulfate in fucosidosis. J Clin Chem Clin Biochem, 1978; 16: 329-334
25) Aibar S, González-Blas CB, Moerman T, Huynh-Thu VA, Imrichova H, Hulselmans G, Rambow F, Marine J-C, Geurts P, Aerts J, Van Den Oord J, Atak ZK, Wouters J, and Aerts S: SCENIC: single-cell regulatory network inference and clustering. Nat Methods, 2017; 14: 1083-1086
26) Milacic M, Beavers D, Conley P, Gong C, Gillespie M, Griss J, Haw R, Jassal B, Matthews L, May B, Petryszak R, Ragueneau E, Rothfels K, Sevilla C, Shamovsky V, Stephan R, Tiwari K, Varusai T, Weiser J, Wright A, Wu G, Stein L, Hermjakob H, and D'Eustachio P: The Reactome Pathway Knowledgebase 2024. Nucleic Acids Research, 2024; 52: D672-D678
27) Bassiouni W, Ali MAM, and Schulz R: Multifunctional intracellular matrix metalloproteinases: implications in disease. The FEBS Journal, 2021; 288: 7162-7182
28) Kelly B, and O'Neill LA: Metabolic reprogramming in macrophages and dendritic cells in innate immunity. Cell Res, 2015; 25: 771-784
29) Thorsten Cramer, Yuji Yamanishi, Björn E. Clausen, Irmgard Förster, Rafal Pawlinski, Nigel Mackman, Volker H. Haase, Rudolf Jaenisch, Maripat Corr, Victor Nizet, Gary S. Firestein, Hans-Peter Gerber, Napoleone Ferrara, and Randall S. Johnson: HIF-1α Is Essential for Myeloid Cell-Mediated Inflammation. Cell, 2003; 112: 645-657
30) Mulder K, Patel AA, Kong WT, Piot C, Halitzki E, Dunsmore G, Khalilnezhad S, Irac SE, Dubuisson A, Chevrier M, Zhang XM, Tam JKC, Lim TKH, Wong RMM, Pai R, Khalil AIS, Chow PKH, Wu SZ, Al-Eryani G, Roden D, Swarbrick A, Chan JKY, Albani S, Derosa L, Zitvogel L, Sharma A, Chen J, Silvin A, Bertoletti A, Blériot C, Dutertre C-A, and Ginhoux F: Cross-tissue single-cell landscape of human monocytes and macrophages in health and disease. Immunity, 2021; 54: 1883-1900.e5
31) An Z, Li J, Yu J, Wang X, Gao H, Zhang W, Wei Z, Zhang J, Zhang Y, Zhao J, and Liang X: Neutrophil extracellular traps induced by IL-8 aggravate atherosclerosis via activation NF-κB signaling in macrophages. Cell Cycle, 2019; 18: 2928-2938
32) Evren E, Ringqvist E, Tripathi KP, Sleiers N, Rives IC, Alisjahbana A, Gao Y, Sarhan D, Halle T, Sorini C, Lepzien R, Marquardt N, Michaëlsson J, Smed-Sörensen A, Botling J, Karlsson MCI, Villablanca EJ, and Willinger T: Distinct developmental pathways from blood monocytes generate human lung macrophage diversity. Immunity, 2021; 54: 259-275.e7
33) Bashore AC, Yan H, Xue C, Zhu LY, Kim E, Mawson T, Coronel J, Chung A, Sachs N, Ho S, Ross LS, Kissner M, Passegué E, Bauer RC, Maegdefessel L, Li M, and Reilly MP: High-Dimensional Single-Cell Multimodal Landscape of Human Carotid Atherosclerosis. ATVB, 2024; 44: 930-945
34) Wiesner P, Choi S-H, Almazan F, Benner C, Huang W, Diehl CJ, Gonen A, Butler S, Witztum JL, Glass CK, and Miller YI: Low Doses of Lipopolysaccharide and Minimally Oxidized Low-Density Lipoprotein Cooperatively Activate Macrophages via Nuclear Factor κ B and Activator Protein-1: Possible Mechanism for Acceleration of Atherosclerosis by Subclinical Endotoxemia. Circulation Research, 2010; 107: 56-65
35) Bae S, Park PSU, Lee Y, Mun SH, Giannopoulou E, Fujii T, Lee KP, Violante SN, Cross JR, and Park-Min K-H: MYC-mediated early glycolysis negatively regulates proinflammatory responses by controlling IRF4 in inflammatory macrophages. Cell Reports, 2021; 35: 109264
36) Ganapathy-Kanniappan S, and Geschwind J-FH: Tumor glycolysis as a target for cancer therapy: progress and prospects. Mol Cancer, 2013; 12: 152
37) Rogers IS, Nasir K, Figueroa AL, Cury RC, Hoffmann U, Vermylen DA, Brady TJ, and Tawakol A: Feasibility of FDG Imaging of the Coronary Arteries. JACC: Cardiovascular Imaging, 2010; 3: 388-397
38) Johnson JL: Metalloproteinases in atherosclerosis. European Journal of Pharmacology, 2017; 816: 93-106
39) Bräuninger H, Krüger S, Bacmeister L, Nyström A, Eyerich K, Westermann D, and Lindner D: Matrix metalloproteinases in coronary artery disease and myocardial infarction. Basic Res Cardiol, 2023; 118: 18
40) Singh P, Sun J, Cavalera M, Al-Sharify D, Matthes F, Barghouth M, Tengryd C, Dunér P, Persson A, Sundius L, Nitulescu M, Bengtsson E, Rattik S, Engelbertsen D, Orho-Melander M, Nilsson J, Monaco C, Goncalves I, and Edsfeldt A: Dysregulation of MMP2-dependent TGF-ß2 activation impairs fibrous cap formation in type 2 diabetes-associated atherosclerosis. Nat Commun, 2024; 15: 10464
41) Jackson V, Olsson T, Kurtovic S, Folkersen L, Paloschi V, Wågsäter D, Franco-Cereceda A, and Eriksson P: Matrix metalloproteinase 14 and 19 expression is associated with thoracic aortic aneurysms. The Journal of Thoracic and Cardiovascular Surgery, 2012; 144: 459-466
42) Lettau I, Hattermann K, Held-Feindt J, Brauer R, Sedlacek R, and Mentlein R: Matrix Metalloproteinase-19 is Highly Expressed in Astroglial Tumors and Promotes Invasion of Glioma Cells. J Neuropathol Exp Neurol, 2010; 69: 215-223
43) Patterson MT, Firulyova MM, Xu Y, Hillman H, Bishop C, Zhu A, Hickok GH, Schrank PR, Ronayne CE, Caillot Z, Fredrickson G, Kennedy AE, Acharya N, Neels JG, Chinetti G, Revelo X, Stromnes IM, Ivanov S, Bold TD, Zaitsev K, and Williams JW: Trem2 promotes foamy macrophage lipid uptake and survival in atherosclerosis. Nat Cardiovasc Res, 2023; 2: 1015-1031
44) Thayaparan D, Emoto T, Khan AB, Besla R, Hamidzada H, El-Maklizi M, Sivasubramaniyam T, Vohra S,

Hagerman A, Nejat S, Needham-Robbins CE, Wang T, Lindquist M, Botts SR, Schroer SA, Taniguchi M, Inoue T, Yamanaka K, Cui H, Al-Chami E, Zhang H, Althagafi MG, Michalski A, McGrath JJC, Cass SP, Luong D, Suzuki Y, Li A, Abow A, Heo R, Pacheco S, Chen E, Chiu F, Byrne J, Furuyashiki T, Husain M, Libby P, Okada K, Howe KL, Heximer SP, Yamashita T, Wang B, Rubin BB, Cybulsky MI, Roy J, Williams JW, Crome SQ, Epelman S, Hirata K, Stampfli MR, and Robbins CS: Endothelial dysfunction drives atherosclerotic plaque macrophage-dependent abdominal aortic aneurysm formation. Nat Immunol, 2025; 26: 706-721

45) Wolak T: Osteopontin - A multi-modal marker and mediator in atherosclerotic vascular disease. Atherosclerosis, 2014; 236: 327-337

46) Zhang H, Liu L, Jiang C, Pan K, Deng J, and Wan C: MMP9 protects against LPS-induced inflammation in osteoblasts. Innate Immun, 2020; 26: 259-269

47) Sasaki S, Nishihira K, Yamashita A, Fujii T, Onoue K, Saito Y, Hatakeyama K, Shibata Y, Asada Y, and Ohbayashi C: Involvement of enhanced expression of classical complement C1q in atherosclerosis progression and plaque instability: C1q as an indicator of clinical outcome. PLoS ONE, 2022; 17: e0262413

Supplemental Methods

ScRNA-seq Data Processing

Analyses were performed using Seurat (v.4.4.0) in an R 4.2.1 environment[1]. (1) Before processing, reads were filtered to remove mitochondrial genes. To exclude doublets and low-quality cells, cells expressing between 300 and 6,000 genes and less than 30% mitochondrial genes for scRNA-seq were picked up and genes expressed in at least 3 cells were used for further analyses. After the selection, Log-normalized with the default parameters. Batch effects were mitigated using Seurat's anchor-based integration across samples. We ran FindIntegrationAnchors with reduction = 'rpca' (dims = [1:40]) and then IntegrateData to generate the integrated assay. For the visualization of the cells in a two-dimensional space, we performed a principal component analysis on the integrated dataset and used the first 40 principal components (PCs) for uniform manifold approximation and projection (UMAP)[2]. We set a parameter resolution 0.3 for scRNA-seq.

We assessed differential gene expressions using non-parametric Wilcoxonranksumtest implemented by Seurat FindAllMarkers function. The top 10 unique differentially expressed genes in each cluster were identified by testing gene expression between each cluster and all other clusters combined and shown as heatmaps in Supple. We identified each cluster based on the unique differentially expressed genes or the expression of the known canonical marker genes by using dot plots or featured plots. We then extracted myeloid cells cluster in scRNA-seq from the integrated dataset and re-clustered them by the same procedure.

RNA Velocity Analyses

In coronary artery plaques dataset, RNA velocity analyses were performed using the velocyto.R program, which is steady-state RNA velocity model[3] with the following parameters: k-NN = 25, deltaT = 1, and gene/fit filters = 0.02. Briefly, Velocity used the raw data to count the spliced (mRNA) and unspliced (Introns) reads for each gene, and generated a.loom file. Those loom files were then loaded into R using read.loom.matrices function to generate a RNA velocity map for spliced and unspliced reads in macrophages in CCS and ACS groups. Estimated velocities were projected onto the UMAP plots. In addition, we note that the steady-state RNA velocity model relies on several assumptions, including approximately constant transcription, splicing, and degradation rates and a near–steady-state relationship between unspliced and spliced mRNA across most genes. These assumptions may be partially violated, particularly in rapidly transitioning cells, and therefore our velocity-based lineage inferences should be interpreted as hypothesis-generating rather than strictly causal.

We also performed RNA velocity analysis with scVelo[4] (version 0.3.3) using its dynamical model. Loom files were imported into AnnData; spliced/unspliced layers were retained and matrices were normalized and log-transformed. We computed first- and second-order moments on the neighborhood graph, then fit gene-wise transcriptional kinetics with scv.tl.recover_dynamics, calculated velocities with scv.tl.velocity(mode = "dynamical"), and built the velocity graph (scv.tl.velocity_graph). Estimated velocities were projected onto the same UMAP embedding used for clustering to ensure comparability across methods, and gene-wise phase portraits were inspected for key drivers. Unless otherwise specified, scVelo default settings were used.

Moreover, we applied all datasets to TFvelo[5]. TFvelo expands RNA velocity concept to various single-cell datasets without relying on splicing information, by introducing gene regulatory information. The Seurat-prepared single-cell data was converted to the Python anaconda data format and merged with the velocity data, allowing the visualization of estimated velocities on UMAP plots.

In addition, we used CellRank[6] (v2.0.7). Velocities (vkey = "velocity") and the expression layer (Ms) were supplied from the scVelo workflow in coronary datasets and TFvelo workflow in carotid datasets. Neighborhood graphs were computed with n_neighbors = 30, n_pcs = 30, and the same UMAP embedding used for clustering was retained for visualization. We built a combined transition kernel as VelocityKernel (weight = 0.9) and ConnectivityKernel (weight = 0.1). We applied the GPCCA estimator and fit macrostates with n_states = 3 (coronary), 14 (carotid). Fate probabilities toward each terminal macrostate were computed and projected onto the UMAP embedding.

Gene Ontology (GO) Analyses

We applied the clusterProfiler package to use gene ontology (GO) analyses for biological process based on the selected differentially expressed genes in macrophages clusters. Specifically, we performed GO over-representation analysis using, for each cluster, upregulated genes identified by Seurat FindMarkers (vs. all other clusters), selecting genes with adjusted p-value <0.05 and average log2FC >0 as input.

Single Cell Metabolic Analysis

Metabolic pathway enrichment was evaluated using single cell scMetabolism[7] and AUCell[8],a computational pipeline for quantifying metabolic change, using the scRNA-seq dataset to elucidate the metabolic landscape of each macrophage sub-cluster.

Statistical Analyses

The Wilcoxon rank-sum test with the Bonferroni correction was performed to calculate q values for comparing gene expressions between ACS and CCS in **Fig.1G**. Differences with $q<0.1$ were considered as significant. Kruskal-Wallis tests followed by Dunn post hocanalysiswereusedto compare gene expressions between each cluster or subcluster in carotid atherosclerosis in Supple (vlnplot). Analyses were performed using Seurat (v.4.4.0) in an R 4.2.1 environment.

Enrollment of Study Participants

For coronary artery disease, we prospectively enrolled CCS/ACS patients undergoing PCI between October 2020 and June 2021 in accordance with AHA/ACC and ESC guidelines. Inclusion criteria were: (i) ACS or CCS without high-intensity signals (HIS) on non-contrast T1-weighted magnetic resonance imaging, and (ii) target lesions with >70% diameter stenosis in large, non-tortuous vessels suitable for DCA (technical details in Supplemental Methods and **Supplemental Fig. 1A, B**). Exclusions: cardiogenic shock, severe CKD (serum creatinine >2.0 mg/dL), and concomitant inflammatory conditions or malignancies. In total, 4 CCS (no HIS) and 6 ACS patients were enrolled; a subset ($n = 3$) was used for scRNA-seq. All participants provided written informed consent. The study complied with the Declaration of Helsinki and was approved by the Ethics Committee of Kobe University and Hyogo Brain and Heart Center (Approval No. B200139) and registered with UMIN Clinical Trials Registry (URL: https://www.umin. ac.jp/ctr; Unique identifier: UMIN000040747).

Public carotid scRNA-seq datasets (GSE253903). We analyzed datasets from GEO. Ethical approvals and informed consent were obtained by the original studies cited with each accession.

References:

1) HaoY, Hao S, Andersen-NissenE, Mauck WM, ZhengS, ButlerA, Lee MJ, WilkAJ, Darby C, Zager M, Hoffman P, Stoeckius M, Papalexi E, Mimitou EP, Jain J, Srivastava A, Stuart T, Fleming LM, Yeung B, Rogers AJ, McElrath JM, Blish CA, Gottardo R, Smibert P, Satija R. Integrated analysis of multimodal single-cell data. Cell, 2021; 184: 3573-3587.e29
2) Becht E, McInnes L, Healy J, Dutertre CA, Kwok IWH, Ng LG, Ginhoux F, NewellEW. Dimensionality reduction for visualizing single-cell data using UMAP. Nat Biotechnol, 2019; 37: 38-44
3) La Manno G, Soldatov R, Zeisel A, Braun E, Hochgerner H, Petukhov V, Lidschreiber K, Kastriti ME, Lönnerberg P, Furlan A, Fan J, Borm LE, Liu Z, Van Bruggen D, Guo J, He X, Barker R, Sundström E, Castelo-Branco G, Cramer P, Adameyko I, Linnarsson S, Kharchenko PV. RNA velocity of single cells. Nature, 2018; 560: 494-498
4) Bergen V, Lange M, Peidli S, Wolf FA, and Theis FJ. Generalizing RNA velocity to transient cell states through dynamical modeling. Nat Biotechnol, 2020; 38: 1408-1414
5) Li J, Pan X, Yuan Y, Shen HB. TFvelo: gene regulation inspired RNA velocity estimation. Nat Commun, 2024; 15: 1387
6) Weiler P, Lange M, Klein M, Pe'er D, and Theis F. CellRank 2: unified fate mapping in multiview single-cell data. Nat Methods, 2024; 21: 1196-1205
7) Wu Y, Yang S, Ma J, Chen Z, Song G, Rao D, Cheng Y, Huang S, Liu Y, Jiang S, Liu J, Huang X, WangX, QiuS, XuJ, XiR, Bai F, ZhouJ, FanJ, ZhangX, GaoQ. SpatiotemporalImmune Landscape of Colorectal Cancer Liver Metastasis at Single-Cell Level. Cancer Discovery, 2022; 12: 134-153
8) Aibar S, González-Blas CB, Moerman T, Huynh-Thu VA, Imrichova H, Hulselmans G, Rambow F, Marine J-C, Geurts P, Aerts J, Van Den Oord J, Atak ZK, Wouters J, and Aerts S. SCENIC: single-cell regulatory network inference and clustering. Nat Methods, 2017; 14: 1083-1086

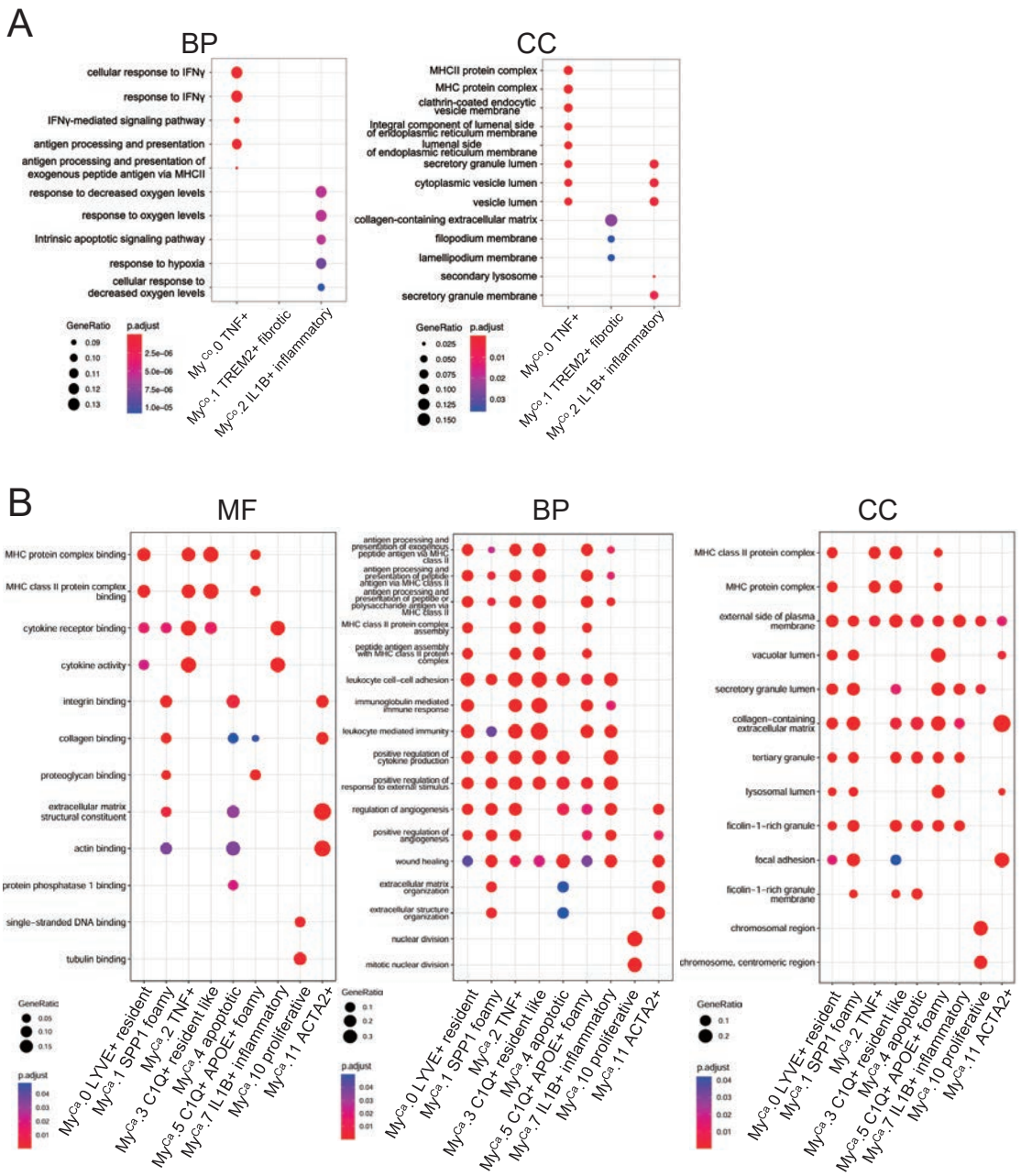

Supplemental Fig. 1. Gene Ontology analyses of macrophages in coronary and carotid plaques

A, Gene Ontology (GO) terms showing enriched biological process (BP) and cell component (CC) of each macrophage subcluster in coronary plaques. B, Gene Ontology (GO) terms showing enriched biological process (BP), molecular function (MF), and cell component (CC) of each macrophage subcluster in carotid plaques.

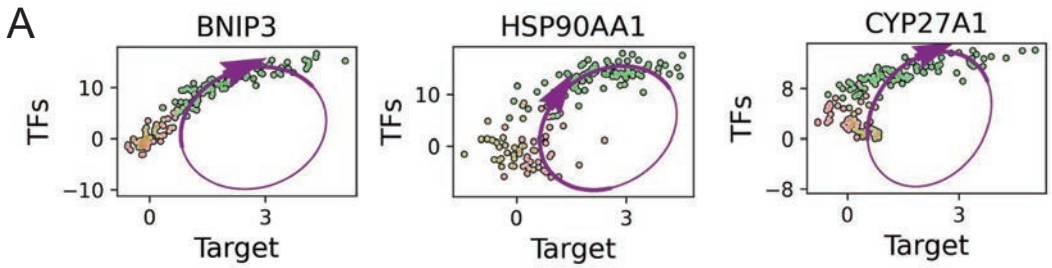

B

Translational factor genes

Target genes	MXI1	EGR1	FOS	CEBPB	ATF3	FOSL2	CEBPD	SPI1	MAFF	KLF4	NR1H3	PPARG	CREM	MBD4	IRF8
BNIP3	0.38279595	0.34789814	-0.22519426	1	-0.24754269	-0.00278257	-0.15500039	-0.28215749	-0.12141485	-0.26849222	-0.05781405	0.0767748	0	0	0
HSP90AA1	-0.16471173	0.26027608	-0.72899964	1	0	0.2156417	0.03739195	-0.01097835	0	0.1736251	0	0.11919105	-0.06834703	0	0
CYP27A1	0.3973218	0	0	0.62694747	0	0	0.48359248	-1	0.23103918	-0.27542253	0	0	0	0.14845502	-0.07716438

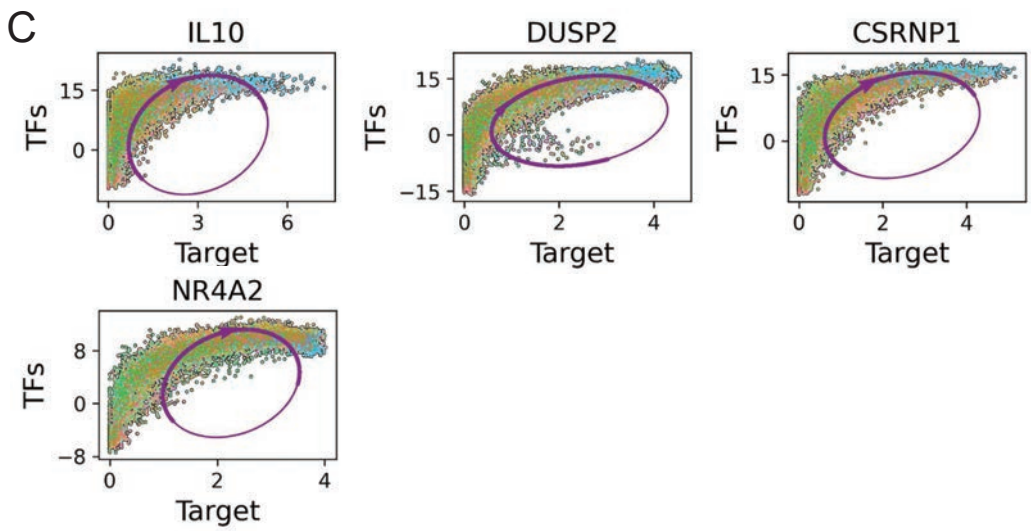

D

Translational factor genes

Target genes	STAT1	FOS	ATF3	KLF4	IRF1	EGR1	MAF	NR1H3	JARID	SMARC	PRDM1	TDRD3	CCND1	SIN3B
IL10	0.24732804	1	0	0.23945068	0.12123327	0.53473782	-0.17394888	0	0	0	0	0	0	0
DUSP2	0.01826264	1	0.31708985	-0.00747241	0	0.33940368	-0.17789277	-0.03195352	-0.03026621	0.04711775	0	0	0	0
NR4A2	0.02381899	1	0.07054254	0.00686843	-0.02033962	0.11706866	0.00745738	0	-0.04663982	0.06163235	-0.10692605	-0.04401787	0.00730358	0.014306
CSRNP1	0.0801546	1	0.23998463	0.19113693	0.09051657	0.26928177	-0.15557394	0	0	0	0	0	0	0.06896694

Supplemental Fig. 2. Transcriptional factor weights estimated by TFvelo revealed a potential driver gene of differentiation toward inflammatory cells

A, Visualization of the phase portrait plots on WX-y space of target genes related inflammation in ACS. B, Visualization of the transcriptional factor weights of target genes related inflammation in ACS. C, Visualization of the phase portrait plots on WX-y
space of target genes related inflammation in symptomatic carotid plaques. D, Visualization of the transcriptional factor weights of target genes related inflammation in symptomatic carotid plaques.

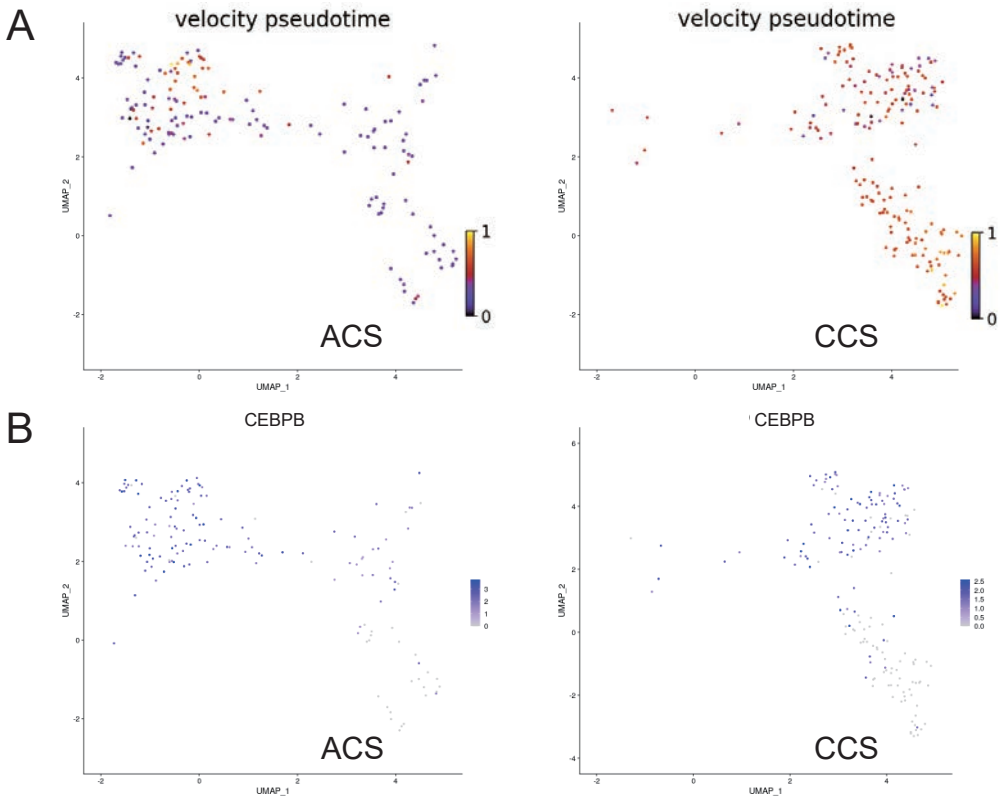

Supplemental Fig. 3. Expression of CEBPB as a potential driver of differentiation toward CXCL3^{+} IL1B^{+} inflammatory macrophages correlated with pseudotime estimated by TFvelo

A, Visualization of pseudotime estimated by TFvelo of coronary artery disease. B, The expression levels of CEBPB gene, separately for ACS and CCS in coronary arteries.

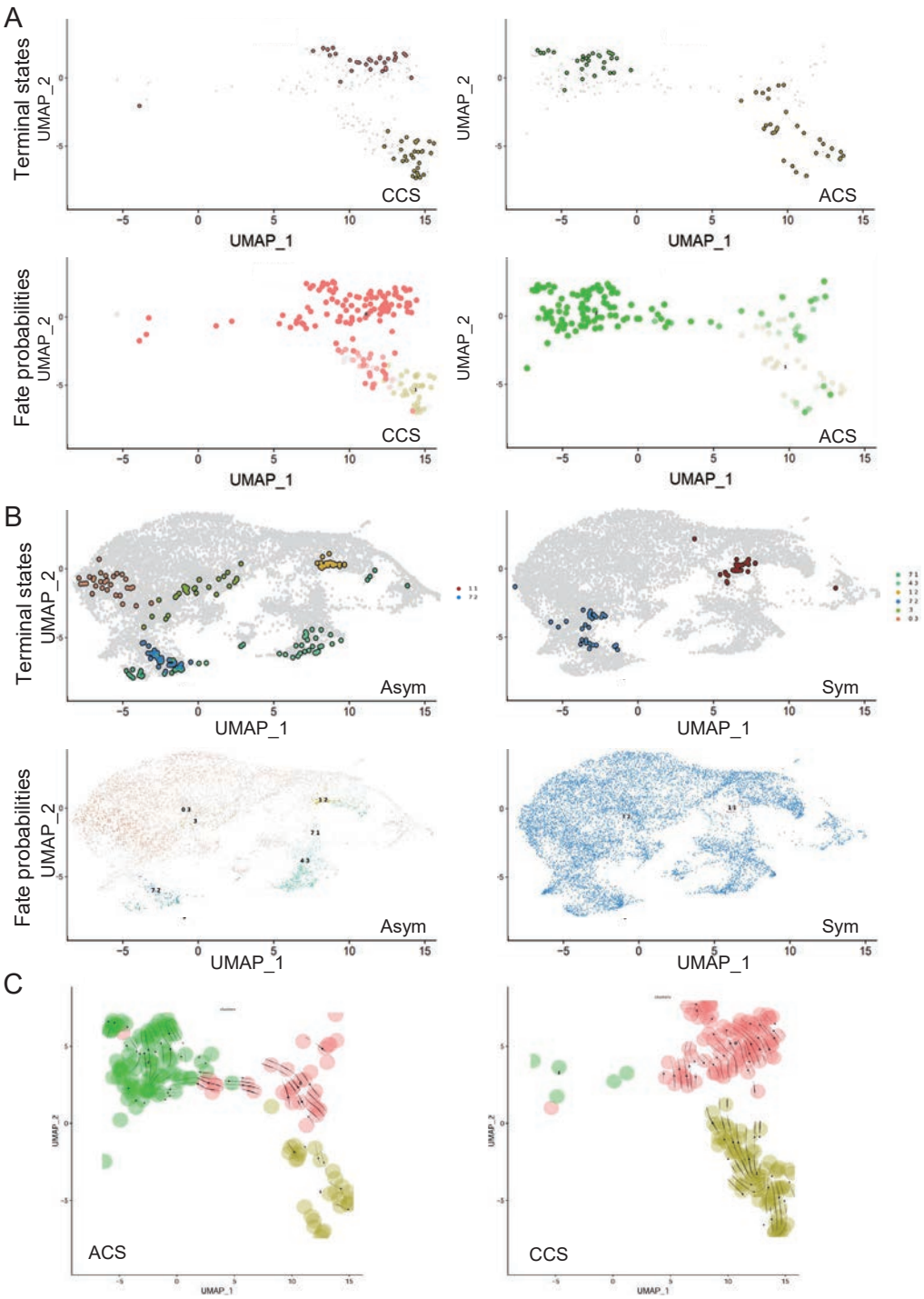

Supplemental Fig. 4. Results of additional cell differentiation analyses

A, Terminal states plot and Fate probabilities plot of CellRank projected to UMAP with macrophage subclusters, separately for ACS and CCS in coronary arteries. B, Terminal states plot and Fate probabilities plot of CellRank projected to UMAP with macrophage subclusters, separately for symptomatic carotid plaques and asymptomatic carotid plaques. C, The velocity stream plot by dynamical model projected to UMAP with macrophage subclusters, separately for ACS and CCS in coronary arteries.

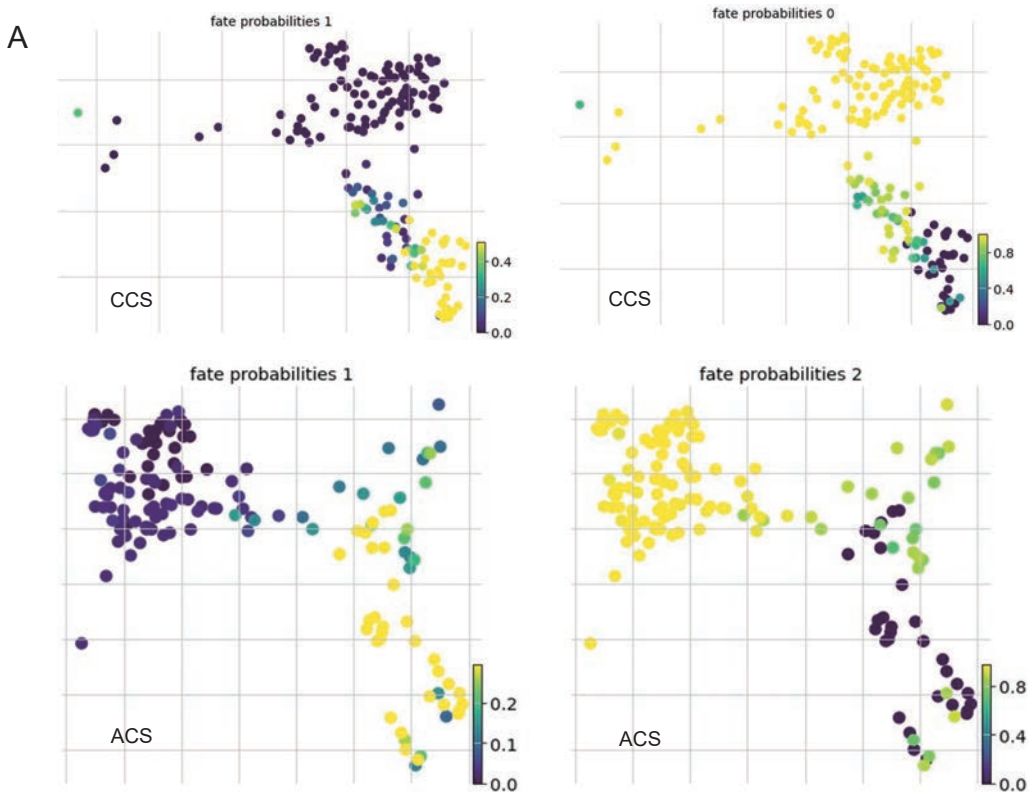

Supplemental Fig. 5. Results of additional cell differentiation analyses

A, Fate probabilities plot of CellRank separately for each terminal states projected to UMAP with macrophage subclusters, separately for ACS and CCS in coronary arteries.

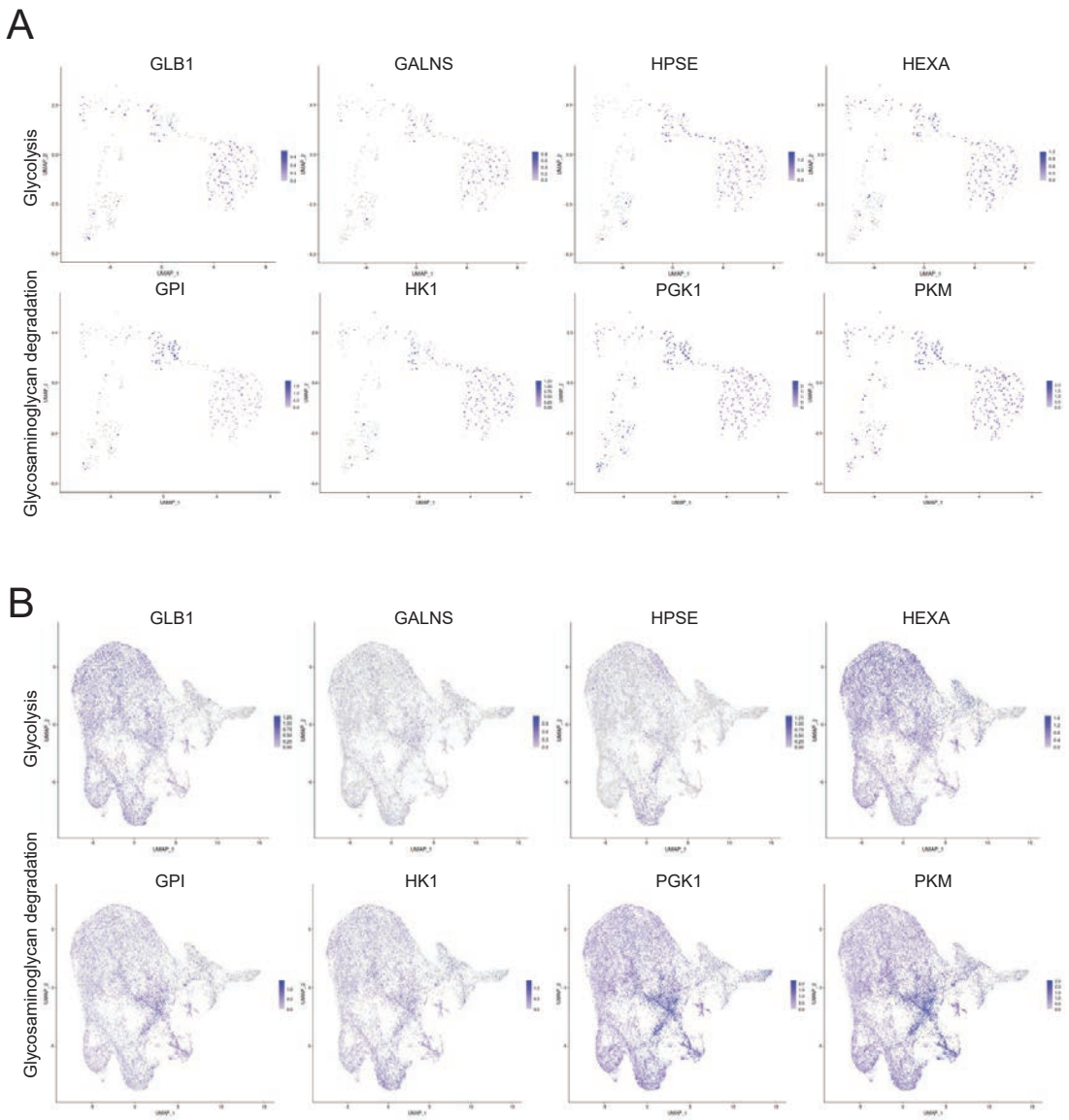

Supplemental Fig. 6. Detected gene expressions related Glycolysis and Glycosaminoglycan degradation pathway correlated with their activation

A, Detected gene expressions related Glycolysis and Glycosaminoglycan degradation pathway in coronary artery disease. B, Detected gene expressions related Glycolysis and Glycosaminoglycan degradation pathway in carotid artery disease.

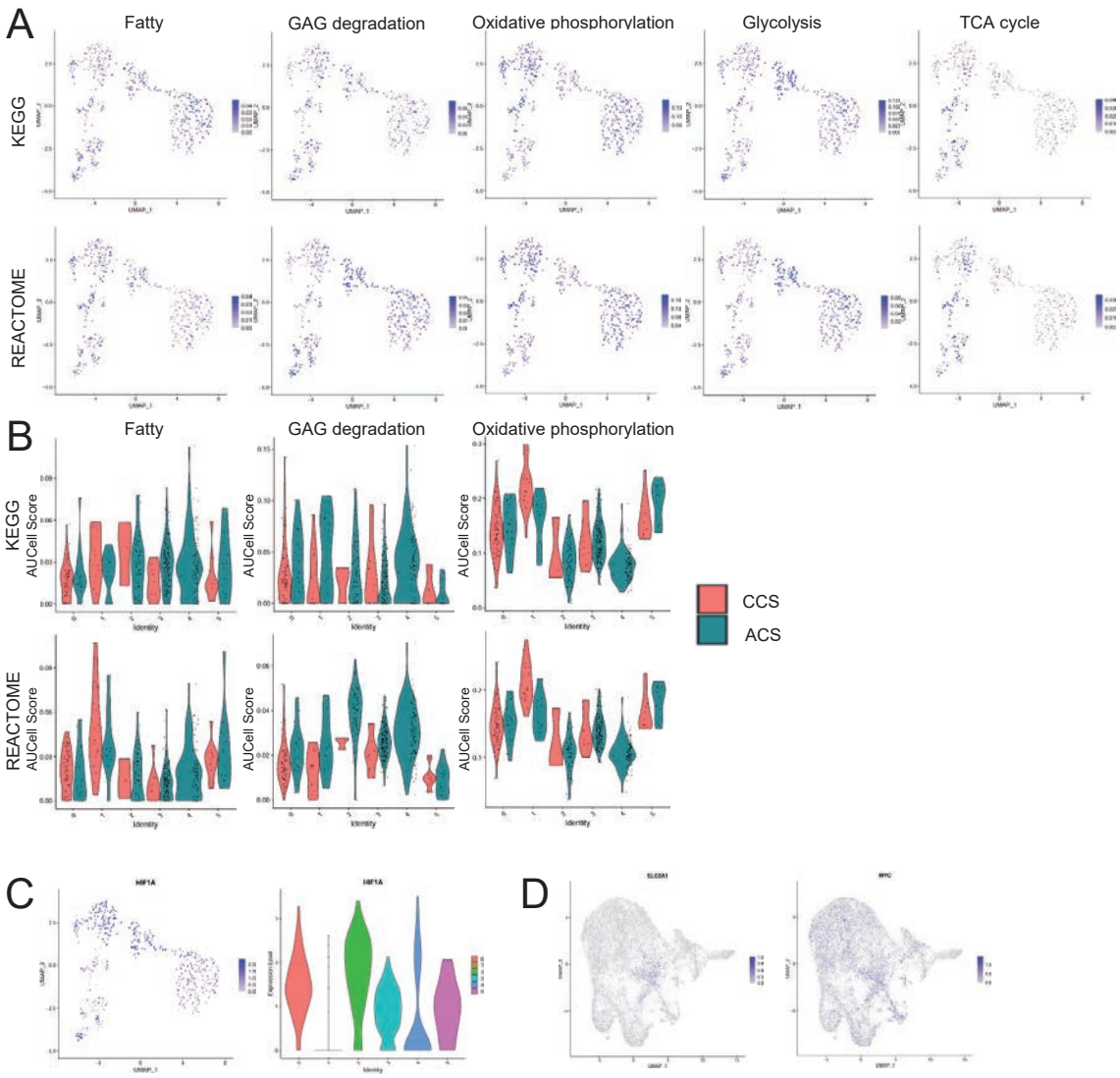

Supplemental Fig. 7. Single-cell metabolic analysis of myeloid cells in carotid artery plaques reveals differentiation between symptomatic and asymptomatic patients

A, Visualization of metabolic analysis results of interesting KEGG and REACTOME pathways by AUCell, separately for ACS and CCS in coronary arteries on UMAP. B, Visualization of metabolic analysis results of interesting KEGG and REACTOME pathways by AUCell, separately for ACS and CCS in coronary arteries. C, Visualization of one of the gene expression regulating glycolysis pathway in coronary artery disease. D, Visualization of gene expressions regulating glycolysis pathway in carotid artery disease.

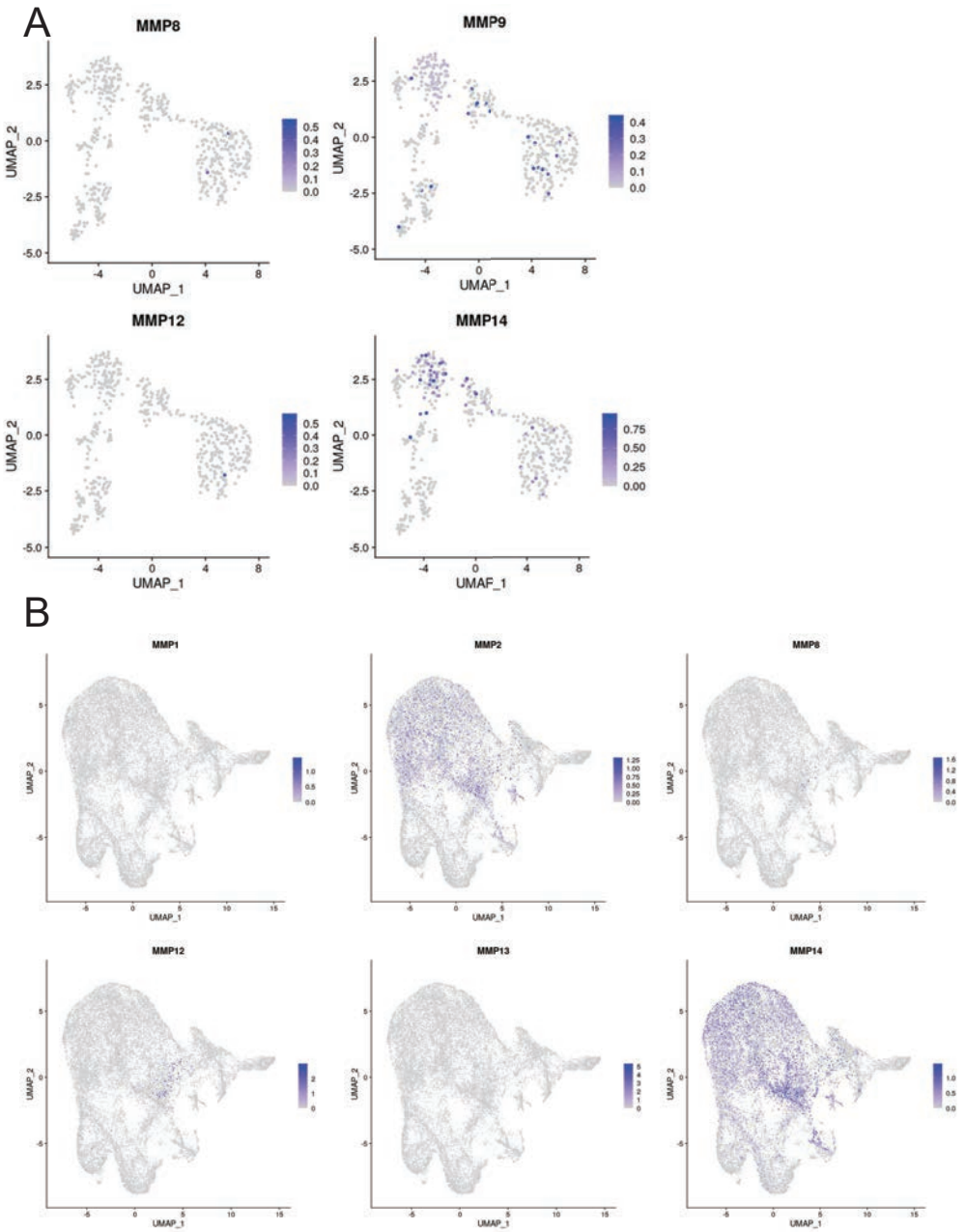

Supplemental Fig. 8. MMPs expression of myeloid cells in coronary and carotid plaques

A, Feature plot depicting the single-cell gene expression related to Glycosaminoglycan degradation (MMP8, MMP9, MMP12, and MMP14) on UMAP in coronary plaques. B, Feature plot depicting the single-cell gene expression related to Glycosaminoglycan degradation (MMP1, MMP2, MMP8, MMP12, MMP13, and MMP14) on UMAP in carotid plaques.

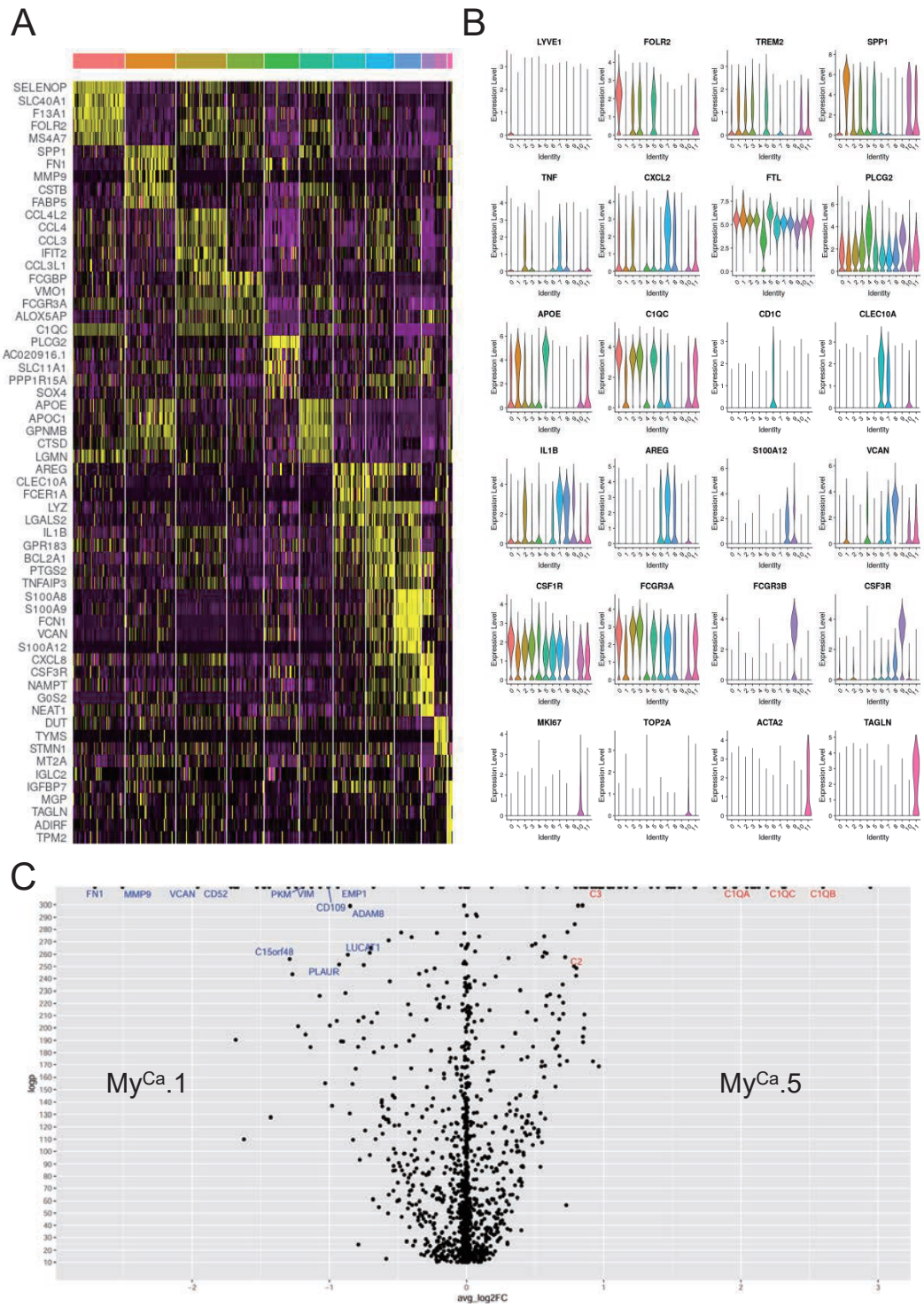

Supplemental Fig. 9. Gene expression of myeloid cell populations in carotid plaques

A, Heat map of the top 5 differentially expressed genes in myeloid cell populations. B, Violin plots depicting single cell gene expression of canonical myeloid cell markers. C, Volcano plot of differentially expressed genes between MyCa.5 and MyCa.1 clusters. Genes highlighted in red have adjusted p value <0.05 and log2 (fold change) ≤ 0.8 and ≥ 0.8.

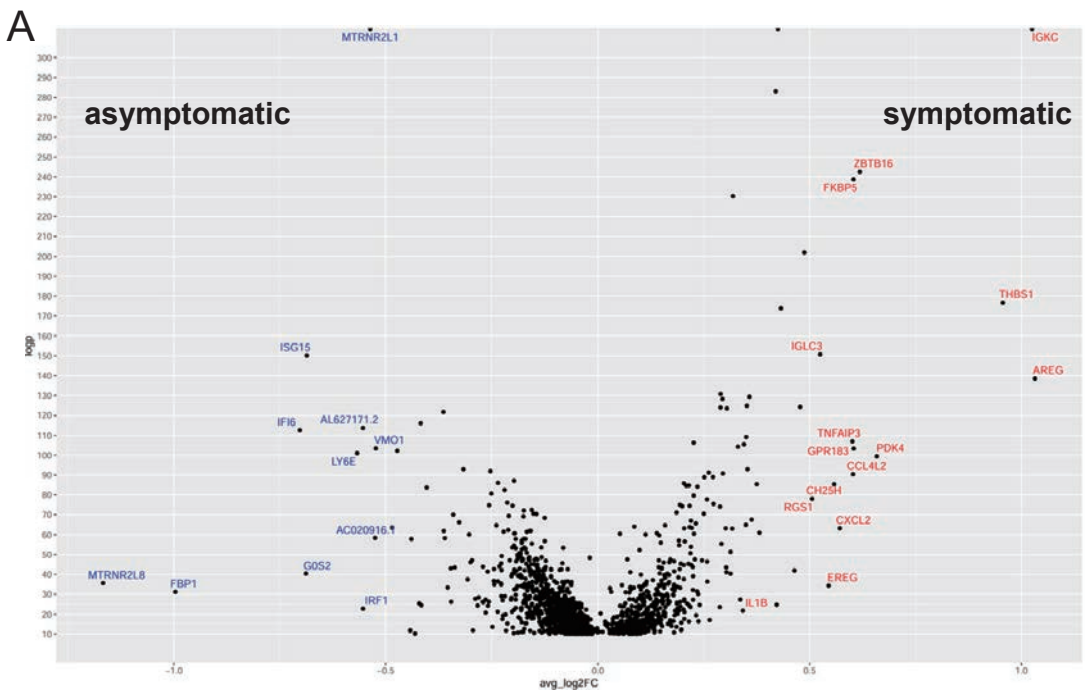

Supplemental Fig. 10. DEG analysis between symptomatic and asymptomatic plaqus reveals higher expression of inflammation-promoting genes in symptomatic plaques than asymptomatic plaques

A, Visualization of DEG analysis result on volcano plot between symptomatic and asymptomatic plaques.

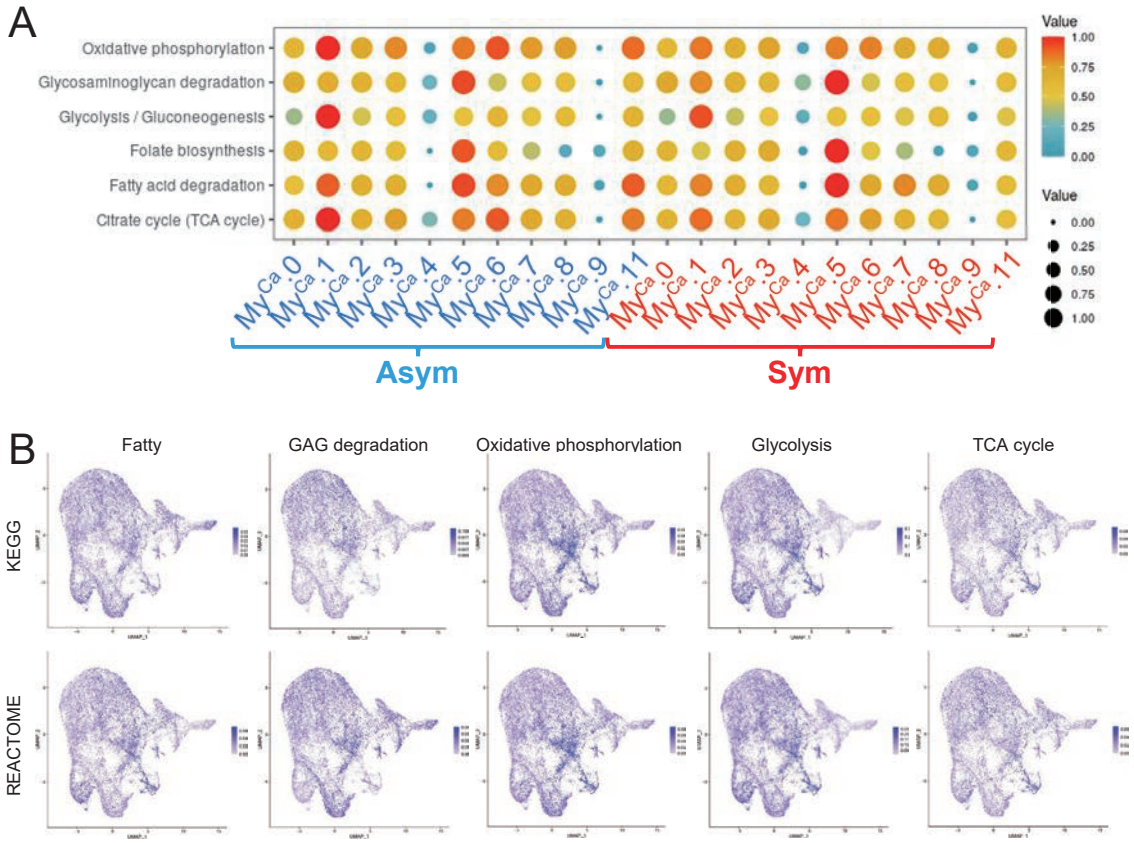

Supplemental Fig. 11. Metabolic analysis results of myeloid cells without proliferative macrophages in carotid plaques

A, Visualization of metabolic analysis results without cluster My.10 (proliferative macrophages) of interesting KEGG pathways by scMetabolism, separately for clusters in symptomatic carotid plaques and asymptomatic carotid plaques on UMAP. B, Visualization of metabolic analysis results of interesting KEGG and REACTOME pathways by AUCell, separately for symptomatic and asymptomatic plaques in carotid arteries on UMAP.